Figure 6. CIN85 knockdown enhances the survival, growth, and differentiation of primary B cells. (A) Control and CIN85-knockdown primary B cells were incubated for 24 hours in medium containing F(ab')2 goat anti–human IgG/IgA/IgM (αIg, 20 μg/mL) or αIg plus CpG (1μM), and CIN85, BcLxL, A1, cyclin D2, and myc mRNA levels were quantified by real-time PCR. The data are normalized to the expression of 18S rRNA. The results shown are representative of 3 independent experiments (*P < .05, **P < .01 vs controls). (B) Control and CIN85-knockdown primary B cells were incubated for 24 hours in the absence or presence of F(ab')2 goat anti–human IgG/IgA/IgM (αIg, 20 μg/mL). The cell lysates were subsequently separated on a SDS-PAGE gel and analyzed by Western blotting with anti-BclxL mAb, anti-cyclin D2 pAb, or anti–β-actin mAb. The resulting values are expressed as fold changes in protein expression compared with nonstimulated control cells. The values are the mean ± SD of 3 independent experiments (**P < .01 vs controls). (C) Control and CIN85-knockdown primary B cells were incubated for 48 hours in the absence or presence of F(ab')2 goat anti–human IgG/IgA/IgM (αIg, 20 μg/mL). After culture, the cells were stained with PE-labeled annexin V and analyzed using flow cytometry. The percentages of annexin-positive cells are shown. A representative histogram of 3 independent experiments is shown. (D) Control and CIN85-knockdown primary B cells were incubated for 48 hours in the absence or presence of F(ab')2 goat anti–human IgG/IgA/IgM (αIg, 20 μg/mL). After culture, the cells were pulsed with BrdU, and its incorporation was detected by incubation with anti-BrdU mAb, followed by rhodamine-conjugated anti–mouse Ab. A representative histogram of 3 independent experiments is shown (**P < .01 vs controls). (E) Control and CIN85-knockdown primary B cells were incubated for 48 hours in the absence or presence of F(ab')2 goat anti–human IgG/IgA/IgM (αIg, 20 μg/mL) and CpG (1μM), and quantitation of Blimp-1 and Xbp-1 mRNA by real-time PCR was carried out. The data are normalized to the expression of 18S rRNA. The results shown are representative of 3 independent experiments (*P < .05 vs controls). (F) Control and CIN85-knockdown primary B cells were incubated for 48 hours with or without F(ab')2 goat anti–human IgG/IgA/IgM (αIg, 20 μg/mL) in the absence or presence of CpG (1μM). The cell lysates were subsequently separated on a SDS-PAGE gel and analyzed by Western blotting with anti–Blimp-1 mAb or anti–β-actin mAb. The resulting values are expressed as fold changes in protein expression compared with unstimulated control cells. The values are the mean ± SD of 3 independent experiments (**P < .01 vs controls).

to compare the roles of CIN85 and CD2AP in the function of human B cells.

BCR signals play a pivotal role in the survival, growth, and differentiation of B cells.[1,2] Under physiologic conditions, BCR signaling is fine-tuned by positive and negative regulators and is generally insufficient for the full activation of B cells, rendering them susceptible to apoptosis and anergy. However, when the negative regulation of BCR signaling is compromised, unwanted B cells could grow and survive, thereby potentially leading to autoimmunity and B-cell malignancies. This study showed that

95

CIN85 knockdown in primary B cells causes full activation of B cells and enhances BCR-induced survival and growth via the increased expression of BcLxL, A1, cyclin D2, and myc (Figure 6). Given that Cbl proteins are critical for B-cell anergy,[10] CIN85 may cooperate with Cbl proteins to function as a key negative regulator for BCR signaling and to maintain self-tolerance. It is thus of interest to determine whether the expression and/or function of CIN85 could be altered in human autoimmune diseases such as SLE. Surprisingly, CLL cells from advanced-stage patients exhibit hypophosphorylation of c-Cbl,[11] as seen in CIN85-knockdown cells. The manipulation of CIN85 expression may therefore provide a novel strategy to control aberrant cell growth and survival in B-cell malignancies.

Acknowledgments

Authorship

Contribution: H.N. and K.A. designed and performed the research, analyzed the data, and wrote the paper; S.J.-T., Y.K., T.S., K.N., S.-i.O., H. Tsuzuki, Y.I., Y.A., H.I., S.S., E.B., H. Tsukamoto, and T.H. performed the research; and T.T. provided cDNA constructs and helped write the paper.

Conflict-of-interest disclosure: The authors declare no competing financial interests.

Correspondence: Hiroaki Niiro, Dept of Medicine and Biosystemic Science, Graduate School of Medical Sciences, Kyushu University, 3-1-1 Maidashi, Higashi-ku, Fukuoka 812-8582, Japan; e-mail: hniiro@med.kyushu-u.ac.jp.

References

1. Niiro H, Clark EA. Regulation of B-cell fate by antigen-receptor signals. *Nat Rev Immunol.* 2002;2(12):945-956.

2. Kurosaki T, Shinohara H, Baba Y. B cell signaling and fate decision. *Annu Rev Immunol.* 2010;28:21-55.

3. Pogue SL, Kurosaki T, Bolen J, Herbst R. B cell antigen receptor-induced activation of Akt promotes B cell survival and is dependent on Syk kinase. *J Immunol.* 2000;165(3):1300-1306.

4. Thien CB, Langdon WY. c-Cbl and Cbl-b ubiquitin ligases: substrate diversity and the negative regulation of signalling responses. *Biochem J.* 2005; 391(pt 2):153-166.

5. Liu YC, Gu H. Cbl and Cbl-b in T-cell regulation. *Trends Immunol.* 2002;23(3):140-143.

6. Swaminathan G, Tsygankov AY. The Cbl family proteins: ring leaders in regulation of cell signaling. *J Cell Physiol.* 2006;209(1):21-43.

7. Duan L, Reddi AL, Ghosh A, Dimri M, Band H. The Cbl family and other ubiquitin ligases: destructive forces in control of antigen receptor signaling. *Immunity.* 2004;21(1):7-17.

8. Panchamoorthy G, Fukazawa T, Miyake S, et al. p120cbl is a major substrate of tyrosine phosphorylation upon B cell antigen receptor stimulation and interacts in vivo with Fyn and Syk tyrosine kinases, Grb2 and Shc adaptors, and the p85 subunit of phosphatidylinositol 3-kinase. *J Biol Chem.* 1996;271(6):3187-3194.

9. Yasuda T, Maeda A, Kurosaki M, et al. Cbl suppresses B cell receptor-mediated phospholipase C (PLC)-gamma2 activation by regulating B cell linker protein-PLC-gamma2 binding. *J Exp Med.* 2000;191(4):641-650.

10. Kitaura Y, Jang IK, Wang Y, et al. Control of the B cell-intrinsic tolerance programs by ubiquitin ligases Cbl and Cbl-b. *Immunity.* 2007;26(5):567-578.

11. Mankai A, Eveillard JR, Buhe V, et al. Is the c-Cbl proto-oncogene involved in chronic lymphocytic leukemia? *Ann N Y Acad Sci.* 2007;1107:193-205.

12. Niiro H, Maeda A, Kurosaki T, Clark EA. The B lymphocyte adaptor molecule of 32 kD (Bam32) regulates B cell antigen receptor signaling and cell survival. *J Exp Med.* 2002;195(1):143-149.

13. Niiro H, Allam A, Stoddart A, Brodsky FM, Marshall AJ, Clark EA. The B lymphocyte adaptor molecule of 32 kilodaltons (Bam32) regulates B cell antigen receptor internalization. *J Immunol.* 2004;173(9):5601-5609.

14. Take H, Watanabe S, Takeda K, Yu ZX, Iwata N, Kajigaya S. Cloning and characterization of a novel adaptor protein, CIN85, that interacts with c-Cbl. *Biochem Biophys Res Commun.* 2000; 268(2):321-328.

15. Gout I, Middleton G, Adu J, et al. Negative regulation of PI 3-kinase by Ruk, a novel adaptor protein. *EMBO J.* 2000;19(15):4015-4025.

16. Bogler O, Furnari FB, Kindler-Roehrborn A, et al. SETA: a novel SH3 domain-containing adapter molecule associated with malignancy in astrocytes. *Neuro Oncol.* 2000;2(1):6-15.

17. Narita T, Amano F, Yoshizaki K, et al. Assignment of SH3KBP1 to human chromosome band Xp22.1->p21.3 by in situ hybridization. *Cytogenet Cell Genet.* 2001;93(1-2):133-134.

18. Petrelli A, Gilestro GF, Lanzardo S, Comoglio PM, Migone N, Giordano S. The endophilin-CIN85-Cbl complex mediates ligand-dependent downregulation of c-Met. *Nature.* 2002;416(6877):187-190.

19. Soubeyran P, Kowanetz K, Szymkiewicz I, Langdon WY, Dikic I. Cbl-CIN85-endophilin complex mediates ligand-induced downregulation of EGF receptors. *Nature.* 2002;416(6877):183-187.

20. Molfetta R, Belleudi F, Peruzzi G, et al. CIN85 regulates the ligand-dependent endocytosis of the IgE receptor: a new molecular mechanism to dampen mast cell function. *J Immunol.* 2005; 175(7):4208-4216.

21. Peruzzi G, Molfetta R, Gasparrini F, et al. The adaptor molecule CIN85 regulates Syk tyrosine kinase level by activating the ubiquitin-proteasome degradation pathway. *J Immunol.* 2007;179(4):2089-2096.

22. Marois L, Vaillancourt M, Pare G, et al. CIN85 modulates the down-regulation of Fc gammaRIIa expression and function by c-Cbl in a PKC-dependent manner in human neutrophils. *J Biol Chem.* 2011;286(17):15073-15084.

23. Tabrizi SJ, Niiro H, Masui M, et al. T cell leukemia/lymphoma 1 and galectin-1 regulate survival/cell death pathways in human naive and IgM+ memory B cells through altering balances in Bcl-2 family proteins. *J Immunol.* 2009;182(3):1490-1499.

24. Narita T, Nishimura T, Yoshizaki K, Taniyama T. CIN85 associates with TNF receptor 1 via Src and modulates TNF-alpha-induced apoptosis. *Exp Cell Res.* 2005;304(1):256-264.

25. Havrylov S, Rzhepetskyy Y, Malinowska A, Drobot L, Redowicz MJ. Proteins recruited by SH3 domains of Ruk/CIN85 adaptor identified by LC-MS/MS. *Proteome Sci.* 2009;7:21.

26. Watanabe S, Take H, Takeda K, Yu ZX, Iwata N, Kajigaya S. Characterization of the CIN85 adaptor protein and identification of components involved in CIN85 complexes. *Biochem Biophys Res Commun.* 2000;278(1):167-174.

27. Chiu CW, Dalton M, Ishiai M, Kurosaki T, Chan AC. BLNK: molecular scaffolding through 'cis'-mediated organization of signaling proteins. *EMBO J.* 2002;21(23):6461-6472.

28. Marshall AJ, Niiro H, Yun TJ, Clark EA. Regulation of B-cell activation and differentiation by the phosphatidylinositol 3-kinase and phospholipase Cgamma pathway. *Immunol Rev.* 2000;176:30-46.

29. Turner M. B-cell development and antigen receptor signalling. *Biochem Soc Trans.* 2002;30(4):812-815.

30. Peng SL, Gerth AJ, Ranger AM, Glimcher LH. NFATc1 and NFATc2 together control both T and B cell activation and differentiation. *Immunity.* 2001;14(1):13-20.

31. Rao N, Ghosh AK, Ota S, et al. The non-receptor tyrosine kinase Syk is a target of Cbl-mediated ubiquitylation upon B-cell receptor stimulation. *EMBO J.* 2001;20(24):7085-7095.

32. Sohn HW, Gu H, Pierce SK. Cbl-b negatively regulates B cell antigen receptor signaling in mature B cells through ubiquitination of the tyrosine kinase Syk. *J Exp Med.* 2003;197(11):1511-1524.

33. Su TT, Rawlings DJ. Transitional B lymphocyte subsets operate as distinct checkpoints in murine splenic B cell development. *J Immunol.* 2002; 168(5):2101-2110.

34. Yi AK, Chang M, Peckham DW, Krieg AM, Ashman RF. CpG oligodeoxyribonucleotides rescue mature spleen B cells from spontaneous apoptosis and promote cell cycle entry. *J Immunol.* 1998;160(12):5898-5906.

35. Calame KL, Lin KI, Tunyaplin C. Regulatory mechanisms that determine the development and function of plasma cells. *Annu Rev Immunol.* 2003;21:205-230.

36. Turner M, Schweighoffer E, Colucci F, Di Santo JP, Tybulewicz VL. Tyrosine kinase SYK: essential functions for immunoreceptor signalling. *Immunol Today.* 2000;21(3):148-154.

37. Stamenova SD, French ME, He Y, Francis SA, Kramer ZB, Hicke L. Ubiquitin binds to and regulates a subset of SH3 domains. *Mol Cell.* 2007; 25(2):273-284.

38. Shimokawa N, Haglund K, Holter SM, et al. CIN85 regulates dopamine receptor endocytosis and governs behaviour in mice. *EMBO J.* 2010; 29(14):2421-2432.

39. Stoddart A, Dykstra ML, Brown BK, Song W, Pierce SK, Brodsky FM. Lipid rafts unite signaling cascades with clathrin to regulate BCR internalization. *Immunity.* 2002;17(4):451-462.

40. Jacob M, Todd L, Sampson MF, Pure E. Dual role of Cbl links critical events in BCR endocytosis. *Int Immunol.* 2008;20(4):485-497.

41. Zhang M, Veselits M, O'Neill S, et al. Ubiquitinylation of Ig beta dictates the endocytic fate of the B cell antigen receptor. *J Immunol.* 2007;179(7): 4435-4443.

42. Oellerich T, Bremes V, Neumann K, et al. The B-cell antigen receptor signals through a preformed transducer module of SLP65 and CIN85. *EMBO J.* 2011;30(17):3620-3634.

43. Kometani K, Yamada T, Sasaki Y, et al. CIN85 drives B cell responses by linking BCR signals to the canonical NF-kappaB pathway. *J Exp Med.* 2011;208(7):1447-1457.

44. Buchse T, Horras N, Lenfert E, et al. CIN85 interacting proteins in B cells-specific role for SHIP-1. *Mol Cell Proteomics.* 2011;10(10):M110.

Intra-Aortic Clusters Undergo Endothelial to Hematopoietic Phenotypic Transition during Early Embryogenesis

Chiyo Mizuochi[1], Stuart T. Fraser[2], Katia Biasch[3], Yuka Horio[1], Yoshikane Kikushige[4], Kenzaburo Tani[5], Koichi Akashi[4], Manuela Tavian[3], Daisuke Sugiyama[1]*

1 Department of Hematopoietic Stem Cells,SSP Stem Cell Unit, Kyushu University Faculty of Medical Sciences, Fukuoka, Japan, 2 Laboratory of Blood Cell Development, Disciplines of Physiology, Anatomy and Histology, School of Medical Sciences, University of Sydney, Camperdown, New South Wales, Australia, 3 Unité 682 INSERM, Strasbourg, France, 4 Department of Medicine and Biosystemic Science, Kyushu University Graduate School of Medical Sciences, Fukuoka, Japan, 5 Department of Molecular Genetics, Medical Institute of Bioregulation, Kyushu University, Fukuoka, Japan

Abstract

Intra-aortic clusters (IACs) attach to floor of large arteries and are considered to have recently acquired hematopoietic stem cell (HSC)-potential in vertebrate early mid-gestation embryos. The formation and function of IACs is poorly understood. To address this issue, IACs were characterized by immunohistochemistry and flow cytometry in mouse embryos. Immunohistochemical analysis revealed that IACs simultaneously express the surface antigens CD31, CD34 and c-Kit. As embryos developed from 9.5 to 10.5 dpc, IACs up-regulate the hematopoietic markers CD41 and CD45 while down-regulating the endothelial surface antigen VE-cadherin/CD144, suggesting that IACs lose endothelial phenotype after 9.5 dpc. Analysis of the hematopoietic potential of IACs revealed a significant change in macrophage CFC activity from 9.5 to 10.5 dpc. To further characterize IACs, we isolated IACs based on CD45 expression. Correspondingly, the expression of hematopoietic transcription factors in the CD45(neg) fraction of IACs was significantly up-regulated. These results suggest that the transition from endothelial to hematopoietic phenotype of IACs occurs after 9.5 dpc.

Introduction

During mouse embryogenesis, hematopoiesis begins at the extra-embryonic yolk sac (YS) at 7.5 days post-coitum (dpc) and shifts to fetal liver after mid-gestation, then to spleen and finally to bone marrow shortly before birth. There are two distinct waves of hematopoietic emergence: a transient wave, primarily restricted to erythropoiesis in YS blood islands prior to the connection of the circulation from the YS to the embryo; and a definitive wave originating in both the YS and embryo proper. The embryonic site has been identified in the aortic region, in the para-aortic splanchnopleura (p-Sp)/aorta-gonad-mesonephros (AGM) region [1–6]. Functional hematopoietic stem cells (HSCs) that can reconstitute adult recipients are first identified in the AGM region at 10.5 dpc after ex vivo organ culture [7]. The cells at 10.5 dpc that were not cultured ex vivo rarely reconstitute adult recipients, whereas those at 11.5 dpc can regardless [7–9]. Therefore, the cells that acquire HSC activity after culture step, have been termed "pre-HSC"s. Although several reports characterize the surface marker expression on both pre-HSCs at 10.5 dpc and HSCs at 11.5 dpc, the developmental process of HSC generation still remains unclear [8–11]. Cell populations capable of reconstituting neonatal recipients are detected in the p-Sp/AGM

region at 9.5 dpc [12–13]. These observations suggest that ancestor cells of HSC from the p-Sp/AGM region at 9.5 dpc require special microenvironments to acquire HSC activity and that HSCs undergo phenotypic changes from 9.5 to 10.5 dpc. In the AGM region, intra-aortic/arterial clusters (IACs) are observed attached to floors of large arteries in several species including chicken, mouse and humans [3]. Mouse IACs have been characterized morphologically and are primarily located in three large arteries, namely, the dorsal aorta (DA), the omphalomesenteric (vitelline) artery (OMA; VA) and the umbilical artery (UA) [3,14–15]. IACs express both hematopoietic (CD41 and CD45) and endothelial (CD31, CD34 and VE-cadherin) surface markers [3,15–16] suggesting that IACs are likely equivalent to ancestor cells of HSC and/or pre-HSCs and are derived from endothelial cells (ECs) at aortic/arterial regions. Although recent genetic approaches and novel tracing methods demonstrate that IACs are derived from ECs in zebrafish and mice, it is unclear how IACs form and acquire HSC activity [17–25].

To address how IACs form and function in HSC generation, we first visualized IACs by immunohistochemistry and confocal imaging and were found to simultaneously express CD31, CD34 and c-Kit. This approach enabled us to investigate the phenotypic
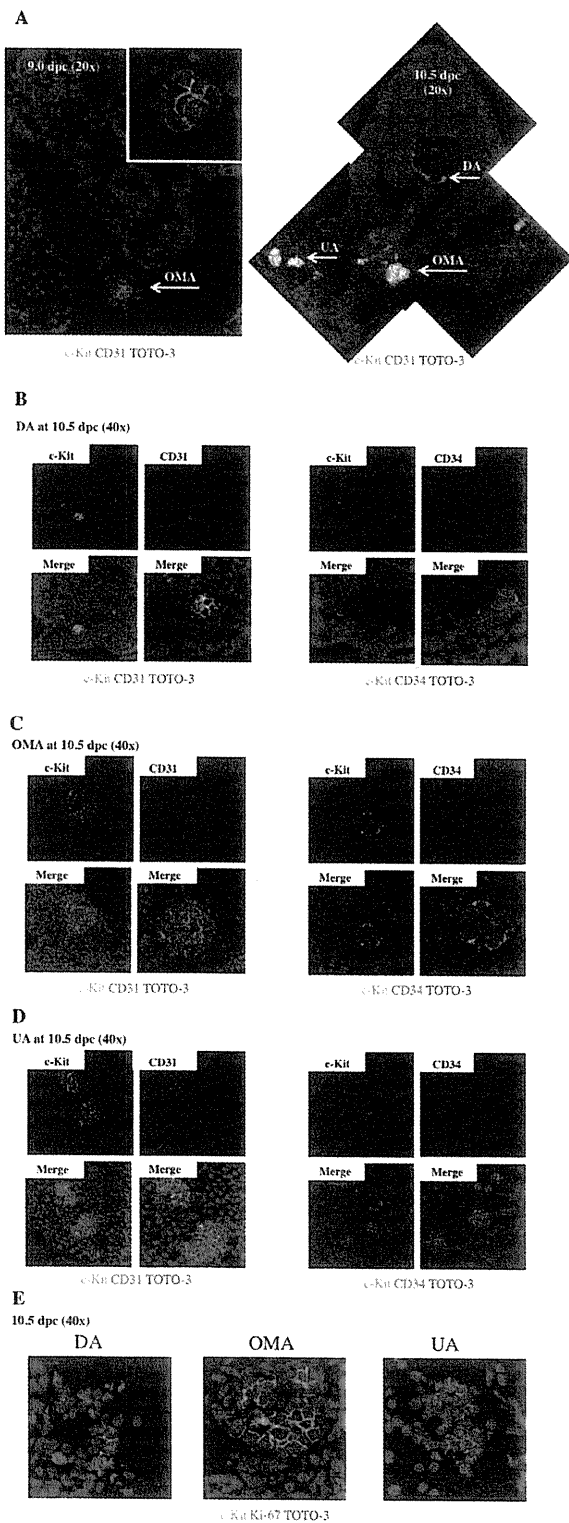
A

B
DA at 10.5 dpc (40x)

C
OMA at 10.5 dpc (40x)

D
UA at 10.5 dpc (40x)

E
10.5 dpc (40x)
DA   OMA   UA

Figure 1. Confocal images of IACs expressing CD31/CD34/c-Kit in the AGM region. Transverse sections of AGM region from ICR mouse embryos at 9.0 and 10.5 dpc were stained with antibodies and observed by confocal microscopy. **(A)** IACs were observed in the omphalomesenteric artery (OMA) at 9.0 dpc (left; magnified view of IACs in upper right panel) and in the OMA, dorsal aorta (DA) and umbilical artery (UA) at 10.5 dpc (right). CD31 (red), c-Kit (green), and TOTO-3 (blue). Arrows indicate IACs. Original magnification is 20x. **(B-D)** IACs were observed in the DA (B), OMA (C) and UA (D) at 10.5 dpc. Left panel shows staining for CD31 (red), c-Kit (green), and TOTO-3 (blue), and right panel shows staining for CD34 (red), c-Kit (green), and TOTO-3 (blue) staining. Images were taken at 40x and zoom was used to show a detail at right lower panel. Another IAC in the DA is shown in Figure S1. **(E)** IACs expressing Ki-67, a marker of proliferation, were observed in the DA (left), OMA (middle) and UA (right). Ki-67 (red), c-Kit (green), and TOTO-3 (blue). Images were taken at 40x and zoom was used to show a detail.
doi:10.1371/journal.pone.0035763.g001

characterization of IACs by flow cytometry and hematopoiesis assays. Here, we demonstrate a significant transition from endothelial to hematopoietic cell phenotype of IAC cells after 9.5 dpc.

Results

Visualization of IACs in mouse embryos

Previous studies identified intra-aortic/arterial clusters (IACs) primarily by immunocytochemistry and microscopy [3,14–15]. Recently, we successfully visualized hematopoietic cell clusters in mouse placenta using thick (20 μm) cryo-sections and antibodies recognizing the embryonic HSC markers c-Kit, CD31 and CD34 and applied this method to quantifying IACs [26]. Cell aggregates consisting of more than three c-Kit-positive cells were defined as an IAC. Here, we used confocal microscopy to expand upon our previous study and characterize the cell types found within IACs according to c-Kit, CD31 and CD34 expression (Figure 1). The first IACs were observed as spherical structures in the omphalo-mesentric artery (OMA) at 9.0 dpc (12–14 somite pairs [SP]) (Figure 1A, left). Between 9.5 dpc (18–22 SP) to 10.5 dpc (30–34 SP), large arteries such as the dorsal aorta (DA), OMA and umbilical artery (UA) form [14]. IACs were observed in DA, OMA and UA at 10.5 dpc, and the size of IACs in the OMA and UA was significantly larger than those seen in the DA (Figure 1A, right). Localization of IACs in DA was not restricted to the ventral wall of DA, but rather some IACs were observed at dorsal and lateral sides of the wall (data not shown). All IACs in the DA, OMA and UA at 10.5 dpc simultaneously expressed c-Kit, CD31 and CD34 (Figure 1B-D). IACs expressing c-Kit in the different arteries analyzed were also positive for Ki-67, a marker of cell proliferation, regardless of location, suggesting that cells within IACs are highly proliferative (Figure 1E).

Characterization of IACs by flow cytometry and hematopoietic progenitor assays

To further characterize IACs, the caudal portion of embryos containing the p-Sp/AGM region was dissociated and analyzed by flow cytometry. At 10.5 dpc, c-Kit$^+$/CD31$^+$/CD34$^+$ cells, which are equivalent to IACs, were assessed for expression of the cell surface markers VE-cadherin/CD144 (an endothelial cell marker), CD41 (the earliest hematopoietic cell marker), CD45 (a pan-leukocyte marker), Sca-1 (a late fetal and adult HSC marker) and CD150 and EPCR (adult HSC markers) (Figure 2A-H). c-Kit$^+$/CD31$^+$/CD34$^+$ cells represented 0.069±0.01% in whole caudal portion of embryos. Among c-Kit$^+$/CD31$^+$/CD34$^+$ cells, VE-cadherin surface antigen expression decreased significantly within 24 hours from 9.5 to 10.5 dpc. Concomitantly, expression of the hematopoietic markers CD41 and CD45 increased from negative or low levels of expression on IAC cells at 9.5 dpc to abundant

99

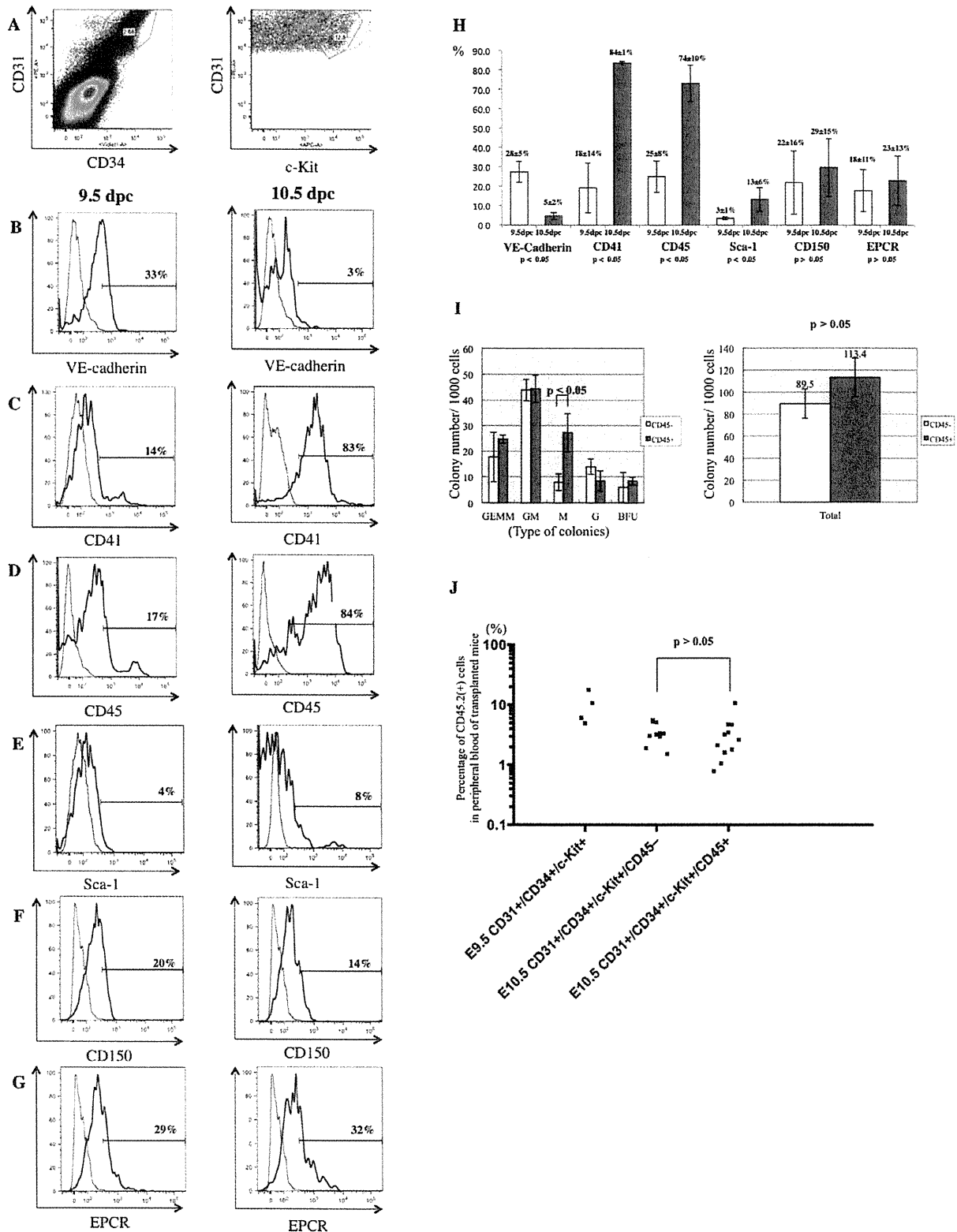**Figure 2. Flow cytometric analysis of CD31⁺/CD34⁺/c-Kit⁺ AGM cells using surface expression of hematopoietic and endothelial cell markers.** Single cell suspensions of the caudal portion of embryos containing the p-Sp/AGM region at 9.5 and 10.5 dpc were prepared and analyzed by flow cytometry. (**A**) Cells expressing CD31, CD34 and c-Kit markers of IACs were gated first. Isotype control of flow cytometric analysis is shown in

Figure S2. (**B–G**) Expression of hematopoietic and endothelial cell markers was analyzed on CD31$^+$/CD34$^+$/c-Kit$^+$ cells at 9.5 dpc (left) and 10.5 dpc (right) with the following antibodies: (**B**) VE-cadherin/CD144 (an endothelial cell marker), (**C**) CD41 (the earliest hematopoietic cell marker), (**D**) CD45 (a pan-leukocyte marker), (**E**) Sca-1 (a late fetal and adult HSC marker), (**F**) CD150 and (**G**) EPCR (adult HSC markers). At least 1,000 cells were assessed for each surface antigen. Representative profiles are shown. (**H**) Percentage of expression was summarized. At least 3 independent experiments were performed. Mean ± 2SD was calculated and shown at the top of bars. (**I**) One thousand sorted CD45-negative or CD45-positive CD31$^+$/CD34$^+$/c-Kit$^+$ cells were cultured in semisolid medium containing the hematopoietic cytokines, SCF (Stem Cell Factor), IL (Interleukin)-3, IL-6 and EPO (Erythropoietin). Left and right panels show each fraction and the total number of colonies, respectively. GEMM (colony-forming units of granulocyte erythrocyte monocyte macrophages); GM (of granulocyte macrophages); M (of macrophages); G (of granulocytes); BFU (burst forming units of erythroid cells). (**J**) 50–100 sorted CD31$^+$/CD34$^+$/c-Kit$^+$ cells at 9.5 dpc, as well as CD45-negative and CD45-positive CD31$^+$/CD34$^+$/c-Kit$^+$ cells were transplanted into busulfan-treated Ly5.1 mouse neonates. Approximately one year after transplantation, blood samples were collected and analyzed for CD45.2 expression by flow cytometry. Representative profile of flow cytometric analysis and its negative and positive controls are shown in Figure S3 and S6, respectively.
doi:10.1371/journal.pone.0035763.g002

levels at 10.5 dpc. Sca-1 expression also increased from 9.5 to 10.5 dpc.

We next separated c-Kit$^+$/CD31$^+$/CD34$^+$ cells based on CD45 expression by flow cytometry and performed colony assays and transplantation assays. As shown in Figure 2I (left), the number of CFU-M generated from CD45-positive c-Kit$^+$/CD31$^+$/CD34$^+$ cells (27.3) was significantly higher than CFU-M from CD45-negative c-Kit$^+$/CD31$^+$/CD34$^+$ cells (8.0) (p<0.05). However, the total number of hematopoietic colonies did not differ between CD45-negative and CD45-positive c-Kit$^+$/CD31$^+$/CD34$^+$ cells (p>0.05). When 50–100 c-Kit$^+$/CD31$^+$/CD34$^+$ cells were transplanted into neonate recipients, there was no significant difference in reconstitution ability (CD45-negative, 3.55%; CD45-positive 3.07%) (p>0.05) (Figure 2J). c-Kit$^+$/CD31$^+$/CD34$^+$ cells at 9.5 dpc were able to reconstitute recipients and chimerism to 9.89% was achieved. Presumptive ancestor cells of HSC can reportedly reconstitute neonate recipients but not adult recipients [13]. In addition, pre-HSCs at 10.5 dpc rarely reconstitute adult recipients without culture step [7–9,11]. When 100 c-Kit$^+$/CD31$^+$/CD34$^+$ cells were transplanted into adult recipients, no reconstitution was observed (data not shown).

Expression of CD45 in mouse and human intra-aortic/arterial clusters

CD45-negative and CD45-positive c-Kit$^+$/CD31$^+$/CD34$^+$ cells showed no difference in hematopoietic potential except within the macrophage lineage. To further investigate a role of CD45 expression on c-Kit$^+$/CD31$^+$/CD34$^+$ cells, we used flow cytometry to segregate c-Kit$^+$/CD31$^+$/CD34$^+$ cells into three fractions. Three distinct populations became apparent; CD45negative cells, CD45low cells, and CD45high cells (Figure 3A). The proportion of CD45-negative and CD45-low positive c-Kit$^+$/CD31$^+$/CD34$^+$ cells was higher at 9.5 dpc than at 10.5 dpc, whereas the percentage of CD45-high positive c-Kit$^+$/CD31$^+$/CD34$^+$ cells increased by 5-fold at 10.5 dpc (31.0%) compared to 9.5 dpc (6.3%) (Figure 3B). These data suggest that CD45-negative c-Kit$^+$/CD31$^+$/CD34$^+$ cells are precursors of CD45-high positive c-Kit$^+$/CD31$^+$/CD34$^+$ cells and that CD45 is a marker of IAC maturation. To address this issue, we examined expression levels of the gene encoding CD45 (*Ptprc; protein tyrosine phosphatase, receptor type, C*) and of various hematopoietic transcription factors (Runx1, c-Myb, Evi-1, SCL and Gata2) (Figure 3C-H). CD45-negative c-Kit$^+$/CD31$^+$/CD34$^+$ cells expressed low levels of *CD45* mRNA. *Ptprc* transcript levels increased significantly as CD45 surface protein expression was up-regulated in the c-Kit$^+$/CD31$^+$/CD34$^+$ population. Expression levels of all hematopoietic transcription factor genes assayed except *Evi-1* was highest in CD45-low positive c-Kit$^+$/CD31$^+$/CD34$^+$ cells. In agreement with flow cytometric analysis, evaluation of CD45 protein expression by immunohistochemistry indicated that IACs in the OMA at 9.5 dpc were CD45-negative while some IACs in the DA, OMA and UA were CD45-positive by 10.5 dpc (Figure 4A-D).

IAC formation in the developing human embryo is poorly defined. Having defined the developmental progression of IAC in the mouse above, we next examined IAC morphology and phenotype in a 32 day-old human embryo. Immunohistochemistry of embryonic human cryosections was performed using anti-human CD34 and CD45 antibodies. As shown in Figure 4E, IACs can be detected in ventral wall of the dorsal aorta. CD34 was expressed by a wide range of vascular endothelial cells throughout the embryo. CD45 was restricted to round and in many cases clearly circulating cells. However, within the IAC observable on the ventral wall of the dorsal aorta, cells expressing both CD34 and CD45 can be seen. This reflects the expression pattern we have identified in embryonic mouse IACs.

Transcription factor hierarchy in IAC development

We next observed IAC formation by immunohistochemistry and flow cytometry in mouse embryos harboring mutations associated with aberrant embryonic hematopoiesis [27–32]. Immunohistochemical analysis of *Runx1$^{-/-}$* embryos lacked IACs in the DA, OMA and UA. Flow cytometric analyses confirmed the absence of c-Kit$^+$/CD31$^+$/CD34$^+$ cells in *Runx1$^{-/-}$* embryos compared to wild type embryos (Figure 5A-B). *Evi-1$^{-/-}$* embryos also lacked IACs in the DA, OMA and UA by immunohistochemistry. However, a small frequency of c-Kit$^+$/CD31$^+$/CD34$^+$ cells could be detected by flow cytometry (Figure 5C). In *c-Myb$^{-/-}$* embryos, IACs were observed at the DA, OMA and UA, and c-Kit$^+$/CD31$^+$/CD34$^+$ cells were also observed by flow cytometry (Figure 5D). Collectively, these results demonstrate that Runx1 is essential for IAC formation while Evi-1 appears to be playing a function downstream of Runx1 in this process.

Discussion

During embryogenesis, a unique cell biological shift takes places in which endothelial cells with adherens junctions detach from each other, alter gene expression and become hematopoietic cells. This process is limited both anatomically and temporally. We here demonstrated that the transition from endothelial to hematopoietic phenotype of IACs occurs from 9.5 dpc in the mouse embryo, earlier than previously described. Furthermore, we show that IACs are identifiable in the human embryo based on CD45 expression, implying that this process in mice is applicable to human.

Previously, we reported an immunohistochemistry visualization technique revealing hematopoietic cell clusters in placenta using thick (20 μm) cryo-sections and antibodies recognizing embryonic HSC markers [26]. Here, we applied this technique to obtain high quality confocal images of intra-aortic/arterial clusters (IACs) in the AGM region. We defined IACs as c-Kit$^+$/CD31$^+$/CD34$^+$ cells. Recently, c-Kit$^+$/CD31$^+$/SSEA-1$^-$ cells were also identified in the AGM region [11]. As CD31 is expressed on both IACs and primordial germ cells (PGCs), it was necessary to exclude PGCs according to SSEA-1 expression. As shown in Figure 2 and 5, we
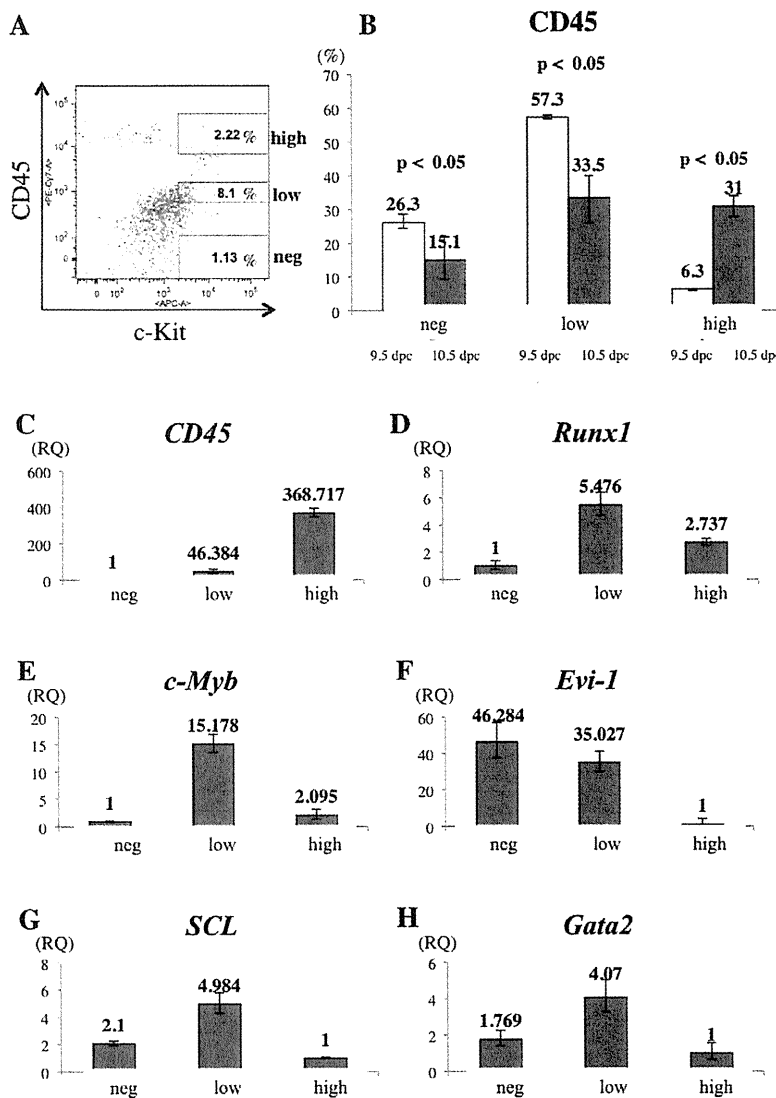
Figure 3. Gene expression analysis in CD31$^+$/CD34$^+$/c-Kit$^+$ AGM cells separated by CD45 expression. (A) Single cell suspensions of the caudal portion of embryos containing the AGM region at 10.5 dpc were prepared and analyzed by flow cytometry. Cells expressing CD31 and CD34, IAC markers, were first gated. The profile shows expression of c-Kit (x-axis) and CD45 (y-axis) in CD31$^+$/CD34$^+$ AGM cells (left). Based on intensity of CD45 expression, CD31$^+$/CD34$^+$/c-Kit$^+$ AGM cells were separated into three fractions, CD45-negative (under 10^2 of CD45-fluorescence, same as negative control), -low positive (from $10^{2.5}$ to $10^{3.5}$ of CD45-fluorescence), and -high positive (approximately over 10^4 of CD45-fluorescence). Isotype control and compensation samples of flow cytometric analysis are shown in Figure S4 and S5. (B) The percentage of CD45-negative, -low positive, and -high positive c-Kit$^+$/CD31$^+$/CD34$^+$ AGM cells was calculated both at 9.5 dpc (white bars) and 10.5 dpc (black bars). (C-H) Gene expression of CD45 (C), Runx1 (D), c-Myb (E), Evi-1 (F), SCL (G) and Gata2 (H) was analyzed in sorted CD45-negative, -low positive and -high positive c-Kit$^+$/CD31$^+$/ CD34$^+$ AGM cells. Expression levels of CD45 mRNA are up-regulated as c-Kit$^+$/CD31$^+$/CD34$^+$ cells express CD45 surface protein. Expression levels of Runx1, c-Myb, Evi-1, SCL and Gata2 were highest in CD45-low positive c-Kit$^+$/CD31$^+$/CD34$^+$ cells, whereas that of Evi-1 was highest in CD45-negative c-Kit$^+$/CD31$^+$/CD34$^+$ cells. RQ represents relative quantity of template in the original sample.
doi:10.1371/journal.pone.0035763.g003

could observe a small number of CD31$^+$/CD34$^-$ cells, which are likely to be PGCs. Since PGCs do not express CD34 at this stage, we could positively select the IAC fraction based on our definition by flow cytometry [33]. Our observation of IACs is compatible with the result showing large IACs were primarily observed in omphalomesentric artery (OMA) and umbilical artery (UA) at 10.5 dpc [11]. In the mouse, IACs protruding into the lumen of arteries were previously reported at 9.5 dpc in studies using microscopy and Tie-

2 immunohistochemistry [14,34]. Prior to 9.5 dpc, we identified the first IACs, which formed a spherical structure, in the OMA at 9.0 dpc (Figure 1A). The OMA appears at 8.0 dpc and directly connects with the dorsal aorta (DA). The OMA anastomoses with the DA after 9.5 dpc and loses its connection with the UA by 10.5 dpc [14,35]. Our data (Figure 1E) indicate that IACs are proliferative, based on Ki-67 staining. Taken together, it is likely that the first IACs in the OMA proliferate and are distributed into
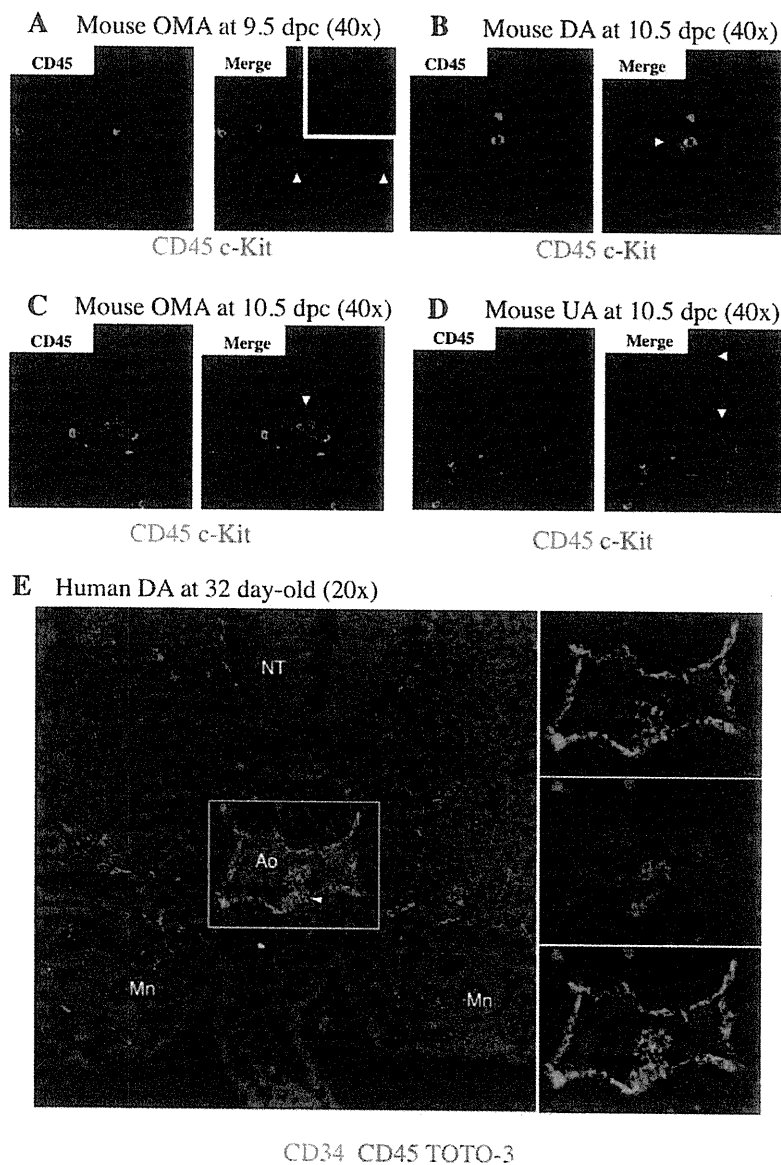
102

Figure 4. Expression of CD45 by mouse and human IACs. Transverse sections of AGM region were made from ICR mouse embryos at 9.5 and 10.5 dpc and from human embryos at 32 day-old, according to the Carnegie classification, stained with antibodies and observed by confocal microscopy. Arrowheads indicate IACs. (**A**) Mouse IACs in the omphalomesenteric artery (OMA) at 9.5 dpc expressed c-Kit, but not CD45. CD45 (green) and c-Kit (red). Magnified view of IACs is shown at right upper panel in Merge panel. Original magnification is 40x. (**B-D**) Mouse IACs in the dorsal aorta (DA) (B), OMA (C) and umbilical artery (UA) (D) at 10.5 dpc expressed c-Kit, and some expressed CD45. CD45 (green) and c-Kit (red). Original magnification is 40x. (**E**) All human IACs in the DA expressed CD34, and some expressed CD45. CD34 (green), CD45 (red) and TOTO-3 (blue). NT (Neural Tube); Ao (Aorta); Mn (Mesonephros). Original magnification is 20x.
doi:10.1371/journal.pone.0035763.g004

large arteries, such as the DA and UA, as the arterial system develops. Although several reports provide direct evidence that endothelial cells (ECs) generate IACs, we cannot rule out the possibility that either mesodermal cells, the ancestors of hematopoietic cells, or so-called hemangioblasts, which give rise both to ECs and hematopoietic cells, generate IACs by another pathway [17–25]. When VE-cadherin$^+$/CD45$^-$ cells were sorted out from AGM regions at 10.5 dpc, and co-aggregated with OP9 stromal cells, these cells acquired HSC activity [8]. As embryos develop,

VE-cadherin$^+$/CD45$^+$ cells from AGM regions at 11.5 dpc can reconstitute adult recipients without culture step, whereas both VE-cadherin$^+$/CD45$^{+/-}$ cells can after aggregation culture with OP9 stromal cells. It suggests that the transition from endothelial to hematopoietic phenotype in pre-HSCs occurs between 10.5 and 11.5 dpc. According to our flow cytometric analysis of IACs, the transition from endothelial to hematopoietic phenotype occurs after 9.5 dpc (Figure 2). Although we found that 33% of c-Kit$^+$/CD31$^+$/CD34$^+$ cells at 9.5 dpc express VE-cadherin, most IACs defined as
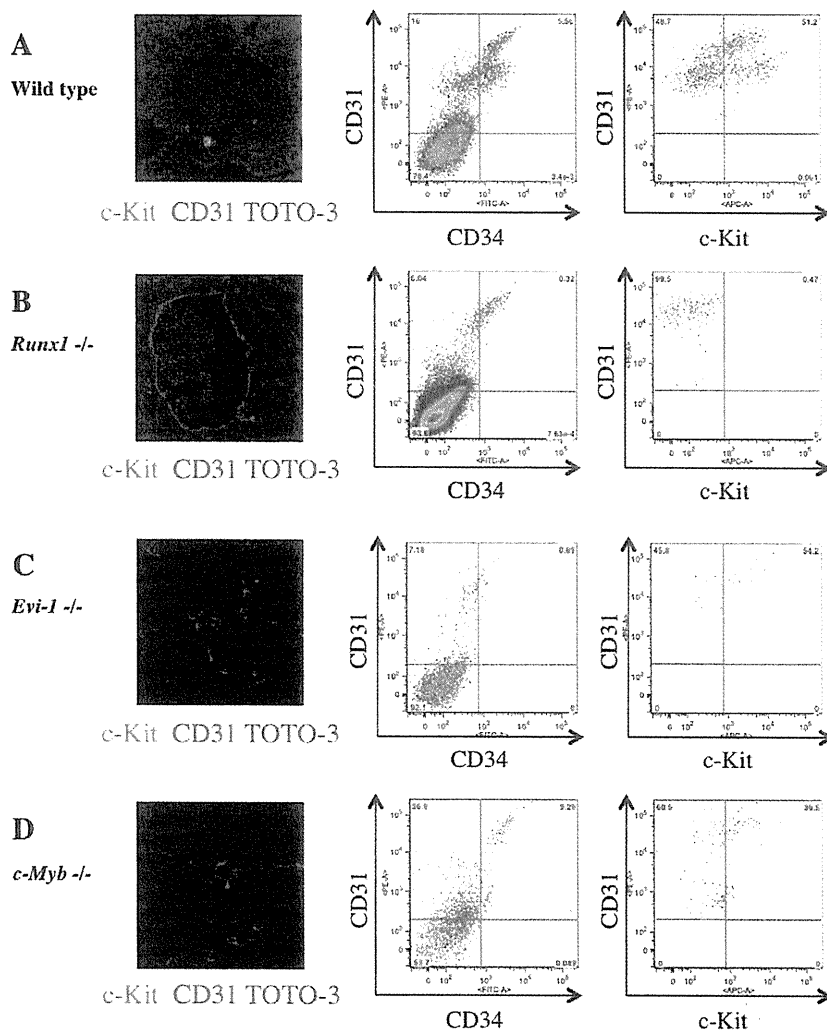
103

Figure 5. Altered IAC phenotype in *Runx1^{-/-}*, *Evi-1^{-/-}* and *c-Myb^{-/-}* embryos. Transverse sections of the AGM region were made from ICR, *Runx1^{-/-}*, *Evi-1^{-/-}* and *c-Myb^{-/-}* mouse embryos at 10.5 dpc, stained with antibodies and observed by confocal microscopy. Single cell suspensions of AGM regions from these embryos at 10.5 dpc were prepared and analyzed by flow cytometry. (**A-D**) Left panels show confocal images stained with anti-c-Kit (green) and CD31 (red) antibodies and TOTO-3 (blue). Middle and right panels show flow cytometric profiles of CD34 (x-axis) and CD31 (y-axis), and c-Kit (x-axis) and CD31 (y-axis), respectively. Isotype control and compensation samples of flow cytometric analysis are shown in Figure S2 and S5. (**A**) ICR mouse embryos serve as (wild type) controls. IACs and CD31$^+$/CD34$^+$/c-Kit$^+$ AGM cells were observed. (**B**) No IACs were observed in *Runx1^{-/-}* embryos, whereas the aortic structure was conserved (left). No CD31$^+$/CD34$^+$/c-Kit$^+$ AGM cells were observed, whereas CD31$^+$/CD34$^+$/c-Kit$^-$ AGM cells, which are equivalent to ECs, were observed (middle and right). (**C**) No IACs were observed and aortic structure was altered in *Evi-1^{-/-}* embryos (left). CD31$^+$ AGM cells were observed, but they did not express CD34 and c-Kit (middle and right). (**D**) IACs were observed in *c-Myb^{-/-}* embryos and the aortic structure was conserved (left). CD31$^+$/CD34$^+$/c-Kit$^+$ AGM cells were observed (middle and right).
doi:10.1371/journal.pone.0035763.g005

c-Kit$^+$/CD31$^+$/CD34$^+$ cells by flow cytometry did not contribute to blood vessel structure. VE-cadherin is expressed in IACs as well as in ECs [16]. It is likely that sorted VE-cadherin$^+$/CD45$^-$ cells from AGM regions at 10.5 dpc contained ECs with HSC potential in addition to some IACs. Further studies are necessary to determine how ECs contribute to IAC generation. CD150 belongs to the SLAM family and its expression is developmentally regulated on the surface of HSCs. At 11.5 dpc, CD150$^-$ cells can reconstitute adult recipients, but CD150$^+$ cells not [10]. In this study, CD150 expression was examined on c-Kit$^+$/CD31$^+$/CD34$^+$ cells by flow cytometry and the percentage of CD150 expression was not

changed (Figure 2F, H). It will be interesting to compare the CD150 expression between 10.5 and 11.5 dpc.

The pan-leukocyte marker CD45 is a transmembrane glycoprotein that functions as a protein phosphotyrosine phosphatase. Although loss of the *CD45* gene results in T and B lymphocyte anomalies in adult, there appears to be no significant abnormality in HSC development during embryogenesis [36–38]. We observed that CD45 protein expression was up-regulated in c-Kit$^+$/CD31$^+$/CD34$^+$ cells between 9.5 and 10.5 dpc (Figure 2D). Our results are compatible with the report showing that CD45 is expressed on the surface of IACs at 10.5 dpc, but not on the IACs at 9.5 dpc [11].

In agreement with previous reports, we observed no significant differences in HSC activity based on neonatal transplantation, whereas myeloid potential differs based on colony formation assay between CD45-negative and CD45-positive c-Kit$^+$/CD31$^+$/CD34$^+$ cells, suggesting that CD45 expression is not required for hematopoietic cell identity (Figure 2I, J) [39–40]. However, pre-HSCs that can reconstitute both adult and neonatal recipients appear at 10.5 dpc, whereas presumptive ancestor cells of HSC that can reconstitute only neonatal but not adult recipients appear at 9.5 dpc [7,12–13]. In accordance with flow cytometric data, some IACs expressed CD45 while others did not in both 10.5 dpc mouse embryos and 32 day-old human embryos (Figure 4B-E). Taken together, although CD45 does not function in HSC development, its expression on the cell surface might serve as a marker of pre-HSC maturation from ancestor cells of HSC. With regard to myeloid potential, only macrophage development differs (Figure 2I). At 10.5 dpc, macrophages are reportedly c-Kit$^-$/CD31$^-$/CD45$^+$ cells, and we could observe some c-Kit$^-$/CD45$^+$ cells in the AGM regions (Figure 4) [11]. CD45 expression on c-Kit$^+$/CD31$^+$/CD34$^+$ cells might be the diverging point of myeloid potential. Furthermore, we identified *CD45* gene expression in CD45-negative c-Kit$^+$/CD31$^+$/CD34$^+$ cells, suggesting that these cells are primed to differentiate into CD45-positive c-Kit$^+$/CD31$^+$/CD34$^+$ cells. Expression levels of *Runx1*, *c-Myb*, *SCL* and *Gata2* were highest in CD45-low positive c-Kit$^+$/CD31$^+$/CD34$^+$ cells, implying that the transition from endothelial to hematopoietic phenotype of IACs occurs in CD45-low positive c-Kit$^+$/CD31$^+$/CD34$^+$ cells, as these transcription factors are reportedly important for the switch to hematopoietic cells [22]. Evi-1 is involved in vasculo-angiogenesis in addition to HSC development [31]. Therefore, high expression level of *Evi-1* gene in CD45-negative c-Kit$^+$/CD31$^+$/CD34$^+$ cells implies that this population still preserves some endothelial identity.

We also investigated IACs from *Runx1*$^{-/-}$, *Evi-1*$^{-/-}$ or *c-Myb*$^{-/-}$ mouse embryos. Runx1 is essential for definitive hematopoiesis, and its expression marks the site of *de novo* generation of definitive hematopoietic cells [28–30]. In agreement with previous reports, we observed an absence of IACs in *Runx1*$^{-/-}$ mouse embryos. Evi-1$^{-/-}$ mouse embryos displayed abnormalities in vascular and hematopoietic development [31–32]. As shown in Figure 5C, *Evi-1*$^{-/-}$ mouse embryos comprised a few c-Kit$^+$/CD31$^+$/CD34$^+$ cells based on flow cytometric analysis. High expression of *Evi-1* in CD45-negative c-Kit$^+$/CD31$^+$/CD34$^+$ cells may correlate with vascular development and impairment of IAC formation. c-Myb is essential for HSC maturation and proliferation, and *c-Myb*$^{-/-}$ mouse embryos die at 15.5 dpc from impaired definitive hematopoiesis in fetal liver, although primitive hematopoiesis appears normal [27]. In contrast to *Runx1*$^{-/-}$ or *Evi-1*$^{-/-}$ mouse embryos, *c-Myb*$^{-/-}$ mouse embryos exhibited IACs.

Several evidences reveal that HSCs are generated from ECs [17–21]. Taken together, our results corroborate HSC-generation from ECs and imply that IACs gradually acquire hematopoietic phenotype after 9.5 dpc. Understanding how IACs are generated could lead to an understanding of how to manipulate HSC generation from ES/iPS cells and thus be applicable to future clinical applications.

Materials and Methods

Mice

Ly5.1 (Sankyo Labo Service, Tokyo, Japan) mice, Ly5.2 adult C57/BL6 mice (Kyudo, Tosu, Japan), ICR mice (SLC, Hamamatsu, Japan), *Runx1*$^{+/-}$ mice (provided by Dr. Speck at University of Pennsylvania), *Evi-1*$^{+/-}$ mice (JAX mice and Services, Bar Harbor, ME) and *c-Myb*$^{+/-}$ mice (JAX mice and Services) were used in these studies. To analyze cells, pregnant mice were sacrificed at 9.0–10.5 dpc and somite pair number was counted. Embryos at 9.0 dpc with 12–14 somite pairs (SP), 9.5 dpc with 18–22 SP and 10.5 dpc with 30–34 SP were dissected out, respectively. Animals were handled according to the Guidelines for the Care and Use of Laboratory Animals of Kyushu University. This study was approved by Animal Care and Use Committee, Kyushu University (Approval ID: A21-068-0).

Mouse immunohistochemistry

Embryos were dissected out and fixed in 2% paraformaldehyde in PBS, followed by equilibration in 30% sucrose in PBS. Embryos were embedded in OCT compound (SAKURA, Tokyo, Japan) and frozen in liquid nitrogen. Tissues were sliced at 20 μm on a Leica CM1900 UV cryostat, transferred to glass slides (Matsunami, Osaka, Japan) and dried thoroughly. Sections were blocked in 1% BSA in PBS and incubated in PBS containing 1% BSA with appropriate dilutions of the following primary antibodies: goat anti-mouse c-Kit (R&D Systems, Minneapolis, MN), rat anti-mouse CD31 (BD Biosciences, San Diego, CA), rat anti-mouse CD34 (BD Biosciences), rat anti-mouse CD45 (Biolegend) and rat anti-mouse Ki-67 antigen (Dako Corporation, Carpinteria, CA) at 4C overnight. After washing in PBS three times, sections were incubated with appropriate dilutions of the following secondary antibodies: Alexa Fluor 488 donkey anti-rat IgG (Invitrogen, Carlsbad, CA), Alexa Fluor 488 donkey anti-goat IgG (Invitrogen), Alexa Fluor 546 donkey anti-goat IgG (Invitrogen) and Alexa Fluor 568 donkey anti-goat IgG (Invitrogen), as well as TOTO-3 (Invitrogen) to stain nuclei, at room temperature for 30 minutes. Samples were mounted on coverslips using fluorescent mounting medium (Dako Corporation) and assessed using a FluoView 1000 confocal microscope (Olympus, Tokyo, Japan).

Human tissues

Human embryos were obtained from voluntary abortions performed according to guidelines and with the approval of the French National Ethics Committee. In all cases, written consent allowing use of the embryo for research was obtained from the patient. Developmental age was estimated based on anatomical criteria and the Carnegie classification as previously described [41–42].

Human immunohistochemistry

Embryos were fixed overnight at 4°C in PBS plus 4% paraformaldehyde (Sigma-Aldrich), rinsed twice in PBS, then in PBS/15% sucrose (Sigma-Aldrich) for at least 24 hours. Tissues were then embedded in PBS with 15% sucrose and 7.5% gelatin (Sigma-Aldrich), frozen and stored at -80°C. Frozen sections (5 μm) were stored at −20°C until use, and then thawed and hydrated in PBS [37]. For double-staining, the TSA Plus Fluorescence amplification system was used, according to the manufacturer's instructions (NEN-Perkin Elmer). Endogenous peroxidases were inhibited for 20 minutes in PBS containing 0.2% hydrogen peroxide (Sigma-Aldrich). Sections were washed in PBS and non-specific binding sites were blocked with PBS/5% goat serum (Vector Laboratories) for 1 hour. Sections were then incubated with uncoupled antibody to CD45 (overnight at room temperature). After rinsing, sections were incubated with biotinylated goat anti-mouse IgG antibody (Immunotech) for 1 hour and then with peroxidase-labeled streptavidin (Immunotech) for 1 hour. Staining was revealed using fluorescent tyramide (TMR, Tetramethylrhodamine). Residual peroxidase activity was inhibited in PBS/0.2% hydrogen peroxide for 10 min at RT. After 3

washings in PBS, slides were treated with an Avidin/Biotin blocking kit according to the manufacturer's instructions (Vector Laboratories). Sections were washed and incubated with anti-CD34 antibody at room temperature for 2 hours, then with biotinylated goat anti-mouse IgG antibody (Immunotech) for 1 hour at RT, and with Alexa 488-labeled streptavidin for 1 hour. Slides were mounted in Vectashield medium (Vector Laboratories). Monoclonal antibodies to CD34 (IgG1, clone Qbend-10) and CD45 (IgG1, clone Hle-1) were purchased from Immunotech and Becton-Dickinson Biosciences, respectively.

Cell preparation

The caudal portion of embryos containing the p-Sp/AGM region was used to obtain a single cell suspension. Tissues were incubated with 1 mg/ml collagenase in medium supplemented with 10% fetal bovine serum for 30 minutes at $37°C$ and filtered through 40-μm nylon cell strainers (BD Biosciences).

Flow cytometry and cell sorting

Antibodies used for analysis were: FITC-conjugated anti-mouse CD41 (eBioscience, San Diego, CA), FITC-conjugated anti-mouse Sca-1 (eBioscience), FITC-conjugated anti-mouse EPCR (Endothelial Protein C Receptor) known as CD201 (Stem Cell Technologies inc, Vancouver, BC), PE-conjugated anti-mouse CD31 (BD Biosciences), PE-Cy7-conjugated anti-mouse CD45 (BioLegend), APC and APC-Cy7-conjugated anti-mouse c-Kit (BD Biosciences), Aexa Fluor488-conjugated anti-mouse CD150 (BioLegend), APC-conjugated anti-mouse VE-cadherin (clone name; VECD-1, provided by Dr. Ogawa at Kumamoto University), and FITC and Pacific Blue-conjugated anti-mouse CD34 (eBioscience). Flow cytometric analysis and cell sorting were carried out using a FACSAria SORP cell sorter (BDIS, San Jose, CA). Data files were analyzed using FlowJo software (Tree Star, Inc., San Carlos, CA).

RNA extraction and real-time PCR analysis

Total RNA was isolated using the RNAqueous 4PCR kit (Ambion Inc., Austin, Texas). mRNA was reverse transcribed using a High-Capacity RNA-to-cDNA kit (Life Technologies, Carlsbad, CA). The quality of cDNA synthesis was evaluated by amplifying mouse ß-actin using PCR. Thirty thermal cycles were used as follows: denaturation at 95°C for 10 sec, annealing at 60°C for 20 sec, followed by extension at 72°C for 20 seconds. Gene expression levels were measured by real time PCR with TaqMan® Gene Expression Master Mix and StepOnePlus™ real time PCR (Life Technologies). All probes were from TaqMan® Gene Expression Assays (Life Technologies). All analyses were performed in triplicate wells; mRNA levels were normalized to ß-actin and the relative quantity (RQ) of expression was compared with a reference sample.

Colony formation assay

Sorted cells were suspended in 3 ml of MethoCult® GF M3434 (Stemcell Technologies) distributed into three 35 mm dishes and then incubated in 5% CO_2 at 37°C. Colonies were counted up 14 days later using an inverted phase contrast microscope CKX41 (Olympus, Tokyo, Japan).

Transplantation assay

To examine neonatal repopulating HSCs, sorted cells were transplanted into busulfan-treated Ly5.1 mouse neonates as described previously [9,15]. Briefly, time-pregnant mice were injected on days 17 and 18 after conception with 15 μg of busulfan/gram body weight of the mother (Sigma-Aldrich, St.Louis MO). Isolated cells were suspended in 25 μl PBS and transplanted into neonates at the time of delivery using a 100 μl Hamilton syringe (Hamilton, Reno, NV). Approximately one year after transplantation, blood samples were collected, lysed in BD Pharm Lyse (BD Biosciences) and analyzed for CD45.2 expression by flow cytometry.

Supporting Information

Figure S1 Additional confocal images of IAC expressing CD31/CD34/c-Kit in the dorsal aorta of AGM region at 10.5 dpc. Staining for CD34 (red), c-Kit (green), and TOTO-3 (blue) is shown. Original magnification is 40x.
(TIFF)

Figure S2 Single cell suspensions of the caudal portion of embryos containing the p-Sp/AGM region at 9.5 and 10.5 dpc were prepared and analyzed by flow cytometry. Upper panels show isotype control of analysis corresponding to Figure 2A. Lower panels show isotype control of analysis corresponding to Figure 5.
(TIFF)

Figure S3 50–100 sorted CD31⁻/CD34⁺/c-Kit⁺ cells at 9.5 dpc, as well as CD45-negative and CD45-positive CD31⁺/CD34⁺/c-Kit⁺ cells were transplanted into busulfan-treated Ly5.1 mouse neonates. Approximately one year after transplantation, blood samples were collected, lysed in lysing solution and analyzed for CD45.2 expression by flow cytometry. Representative profile of flow cytometric analysis is shown.
(TIFF)

Figure S4 Single cell suspensions of the caudal portion of embryos containing the AGM region at 10.5 dpc were prepared and analyzed by flow cytometry. The profile shows isotype control of analysis corresponding to Figure 3A. Based on the isotype control, sorting gates are set into three fractions, CD45-negative (under 10^2 of CD45-fluorescence, same as negative control), -low positive (from $10^{2.5}$ to $10^{3.5}$ of CD45-fluorescence), and -high positive (approximately over 10^4 of CD45-fluorescence).
(TIFF)

Figure S5 Single cell suspensions of the caudal portion of embryos containing the p-Sp/AGM region at 9.5 and 10.5 dpc were prepared and analyzed by flow cytometry. Compensation samples of analysis corresponding to Figure 3A and 5 were shown.
(TIFF)

Figure S6 Negative and positive controls to transplantation analysis are shown corresponding to Figure S3. Peripheral blood samples were obtained from Ly5.1 adult mouse for negative control and Ly5.2 adult C57/BL6 mice for positive control, respectively.
(TIFF)

Acknowledgments

106

Author Contributions

Conceived and designed the experiments: DS. Performed the experiments: CM KB YH YK MT DS. Analyzed the data: CM SF KB MT DS.

Contributed reagents/materials/analysis tools: CM KB MT KT KA DS. Wrote the paper: CM SF DS.

References

1. Dzierzak E, Speck NA (2008) Of lineage and legacy: the development of mammalian hematopoietic stem cells. Nat Immunol 9: 129–136.
2. Mikkola HK, Orkin SH (2006) The journey of developing hematopoietic stem cells. Development 133: 3733–3744.
3. Godin I, Cumano A (2002) The hare and the tortoise: an embryonic haematopoietic race. Nat Rev Immunol 2: 593–604.
4. Dieterlen-Lievre F, Pouget C, Bollerot K, Jaffredo T (2006) Are intra-aortic hemopoietic cells derived from endothelial cells during ontogeny? Trends Cardiovasc Med 16: 128–139.
5. Jaffredo T, Bollerot K, Sugiyama D, Gautier R, Drevon C (2005) Tracing the hemangioblast during embryogenesis: developmental relationships between endothelial and hematopoietic cells. Int J Dev Biol 49: 269–277.
6. Sugiyama D, Tsuji K (2006) Definitive hematopoiesis from endothelial cells in the mouse embryo; a simple guide. Trends Cardiovasc Med 16: 45–49.
7. Medvinsky A, Dzierzak E (1996) Definitive hematopoiesis is autonomously initiated by the AGM region. Cell 86: 897–906.
8. Taoudi S, Gonneau C, Moore K, Sheridan JM, Blackburn CC, et al. (2008) Extensive hematopoietic stem cell generation in the AGM region via maturation of VE-cadherin+CD45+ pre-definitive HSCs. Cell Stem Cell 3: 99–108.
9. Rybtsov S, Sobiesiak M, Taoudi S, Souilhol C, Senserrich J, et al. (2011) Hierarchical organization and early hematopoietic specification of the developing HSC lineage in the AGM region. J Exp Med 208: 1305–1315.
10. McKinney-Freeman SL, Naveiras O, Yates F, Loewer S, Philitas M, et al. (2009) Surface antigen phenotypes of hematopoietic stem cells from embryos and murine embryonic stem cells. Blood 114: 268–278.
11. Yokomizo T, Dzierzak E (2010) Three-dimensional cartography of hematopoietic clusters in the vasculature of whole mouse embryos. Development 137: 3651–3661.
12. Kumano K, Chiba S, Kunisato A, Sata M, Saito T, et al. (2003) Notch1 but not Notch2 is essential for generating hematopoietic stem cells from endothelial cells. Immunity 18: 699–711.
13. Yoder MC, Hiatt K, Dutt P, Mukherjee P, Bodine DM, et al. (1997) Characterization of definitive lymphohematopoietic stem cells in the day 9 murine yolk sac. Immunity 7: 335–344.
14. Garcia-Porrero JA, Godin IE, Dieterlen-Lievre F (1995) Potential intraembryonic hemogenic sites at pre-liver stages in the mouse. Anat Embryol (Berl) 192: 425–435.
15. Garcia-Porrero JA, Manaia A, Jimeno J, Lasky LL, Dieterlen-Lievre F, et al. (1998) Antigenic profiles of endothelial and hemopoietic lineages in murine intraembryonic hemogenic sites. Dev Comp Immunol 22: 303–319.
16. Fraser ST, Ogawa M, Yokomizo T, Ito Y, Nishikawa S (2003) Putative intermediate precursor between hematogenic endothelial cells and blood cells in the developing embryo. Dev Growth Differ 45: 63–75.
17. Jaffredo T, Gautier R, Eichmann A, Dieterlen-Lievre F (1998) Intraaortic hemopoietic cells are derived from endothelial cells during ontogeny. Development 125: 4575–4583.
18. Sugiyama D, Ogawa M, Hirose I, Jaffredo T, Arai K, et al. (2003) Erythropoiesis from acetyl LDL incorporating endothelial cells at the preliver stage. Blood 101: 4733–4738.
19. Sugiyama D, Arai K, Tsuji K (2005) Definitive hematopoiesis from acetyl LDL incorporating endothelial cells in the mouse embryo. Stem Cells Dev 14: 687–696.
20. Bertrand JY, Giroux S, Golub R, Klaine M, Jalil A, et al. (2005) Characterization of purified intraembryonic hematopoietic stem cells as a tool to define their site of origin. Proc Natl Acad Sci U S A 102: 134–139.
21. Zovein AC, Hofmann JJ, Lynch M, French WJ, Turlo KA, et al. (2008) Fate tracing reveals the endothelial origin of hematopoietic stem cells. Cell Stem Cell 3: 625–636.
22. Chen MJ, Yokomizo T, Zeigler BM, Dzierzak E, Speck NA (2009) Runx1 is required for the endothelial to haematopoietic cell transition but not thereafter. Nature 457: 887–891.
23. Bertrand JY, Chi NC, Santoso B, Teng S, Stainier DY, et al. (2010) Haematopoietic stem cells derive directly from aortic endothelium during development. Nature 464: 108–111.
24. Kissa K, Herbomel P (2010) Blood stem cells emerge from aortic endothelium by a novel type of cell transition. Nature 464: 112–115.
25. Boisset JC, van Cappellen W, Andrieu-Soler C, Galjart N, Dzierzak E, et al. (2010) In vivo imaging of haematopoietic cells emerging from the mouse aortic endothelium. Nature 464: 116–120.
26. Sasaki T, Mizuochi C, Horio Y, Nakao K, Akashi K, et al. (2010) Regulation of hematopoietic cell clusters in the placental niche through SCF/Kit signaling in embryonic mouse. Development 137: 3941–3952.
27. Mucenski ML, McLain K, Kier AB, Swerdlow SH, Schreiner CM, et al. (1991) A functional c-myb gene is required for normal murine fetal hepatic hematopoiesis. Cell 65: 677–689.
28. Okuda T, van Deursen J, Hiebert SW, Grosveld G, Downing JR (1996) AML1, the target of multiple chromosomal translocations in human leukemia, is essential for normal fetal liver hematopoiesis. Cell 84: 321–330.
29. Wang Q, Stacy T, Binder M, Marin-Padilla M, Sharpe AH, et al. (1996) Disruption of the Cbfa2 gene causes necrosis and hemorrhaging in the central nervous system and blocks definitive hematopoiesis. Proc Natl Acad Sci U S A 93: 3444–3449.
30. North T, Gu TL, Stacy T, Wang Q, Howard L, et al. (1999) Cbfa2 is required for the formation of intra-aortic hematopoietic clusters. Development 126: 2563–2575.
31. Yuasa H, Oike Y, Iwama A, Nishikata I, Sugiyama D, et al. (2005) Oncogenic transcription factor Evi1 regulates hematopoietic stem cell proliferation through GATA-2 expression. EMBO J 24: 1976–1987.
32. Goyama S, Yamamoto G, Shimabe M, Sato T, Ichikawa M, et al. (2008) Evi-1 is a critical regulator for hematopoietic stem cells and transformed leukemic cells. Cell Stem Cell 3: 207–220.
33. Wood HB, May G, Healy L, Enver T, Morris-Kay GM (1997) CD34 expression patterns during early mouse development are related to modes of blood vessel formation and reveal additional sites of hematopoiesis. Blood 90: 2300–2311.
34. Takakura N, Huang XL, Naruse T, Hamaguchi I, Dumont DJ, et al. (1998) Critical role of the TIE2 endothelial cell receptor in the development of definitive hematopoiesis. Immunity 9: 677–686.
35. Theiler K (1972) The house mouse: development and normal stages from fertilization to 4 weeks of age. Springer, Berlin Heidelberg New York.
36. Kishihara K, Penninger J, Wallace VA, Kundig TM, Kawai K, et al. (1993) Normal B lymphocyte development but impaired T cell maturation in CD45-exon6 protein tyrosine phosphatase-deficient mice. Cell 74: 143–156.
37. Byth KF, Conroy LA, Howlett S, Smith AJ, May J, et al. (1996) CD45-null transgenic mice reveal a positive regulatory role for CD45 in early thymocyte development, in the selection of CD4+CD8+ thymocytes, and B cell maturation. J Exp Med 183: 1707–1718.
38. Mee PJ, Turner M, Basson MA, Costello PS, Zamoyska R, et al. (1999) Greatly reduced efficiency of both positive and negative selection of thymocytes in CD45 tyrosine phosphatase-deficient mice. Eur J Immunol 29: 2923–2933.
39. North TE, de Bruijn MF, Stacy T, Talebian L, Lind E, et al. (2002) Runx1 expression marks long-term repopulating hematopoietic stem cells in the midgestation mouse embryo. Immunity 16: 661–672.
40. Matsubara A, Iwama A, Yamazaki S, Furuta C, Hirasawa R, et al. (2005) Endomucin, a CD34-like sialomucin, marks hematopoietic stem cells throughout development. J Exp Med 202: 1483–1492.
41. O'Rahilly R, Muller F (1987) Development Stages in Human Embryos. Washington: Carnegie Institution of Washington.
42. Tavian M, Peault B (2005) The changing cellular environments of hematopoiesis in human development in utero. Exp Hematol 33: 1062–1069.

Different Risk Factors Related to Adenovirus- or BK Virus-Associated Hemorrhagic Cystitis following Allogeneic Stem Cell Transplantation

Yasuo Mori,[1,2] Toshihiro Miyamoto,[1] Koji Kato,[1] Kenjiro Kamezaki,[1] Takuro Kuriyama,[1] Seido Oku,[1] Katsuto Takenaka,[1] Hiromi Iwasaki,[2] Naoki Harada,[1] Motoaki Shiratsuchi,[3] Yasunobu Abe,[3] Koji Nagafuji,[1] Takanori Teshima,[2] Koichi Akashi[1,2]

Virus-associated hemorrhagic cystitis (HC) is a major cause of morbidity and mortality following allogeneic hematopoietic stem cell transplantation (HSCT). Although numerous studies have attempted to identify factors that predispose patients to viral HC, its causes remain controversial. We analyzed retrospectively the results of 266 allogeneic HSCTs to identify factors associated with HC. Of this group, 42 patients (15.8%) were diagnosed with viral HC, because of either adenovirus (ADV; n = 26; 9.8%) or BK virus (BKV; n = 16; 6.0%). ADV-HC was frequently associated with T cell purging, and was less common in patients with acute graft-versus-host-disease (GVHD). Conversely, BKV-HC was more frequently observed in patients with excessive immune reactions such as GVHD, preengraftment immune reaction, and hemophagocytic syndrome. These observations indicate that ADV- and BKV-HC may differ significantly in their risk factors and pathogenesis. Profound immune deficiency is more likely to be associated with ADV-HC, whereas immune hyperactivity might play a key role in BKV-HC.

Biol Blood Marrow Transplant 18: 458-465 (2012) © 2012 American Society for Blood and Marrow Transplantation

KEY WORDS: Hemorrhagic cystitis, Adenovirus, BK virus, Stem cell transplantation, Immune reaction

INTRODUCTION

Hemorrhagic cystitis (HC) is one of the most common complications following hematopoietic stem cell transplantation (HSCT), which remarkably decreases patients' quality of life, and potentially causes therapy-related mortality [1-3]. Clinical manifestations of HC vary from painless microscopic hematuria to gross hematuria, clot formation within the urinary tract, and obstructive renal failure [4]. Early-onset HC that occurs during or shortly after high-dose chemotherapy as part of the conditioning regimen is generally

related to cyclophosphamide (CY) toxicity, whereas late-onset HC is mainly attributed to viral infection. BK virus (BKV) is most frequently associated with late-onset HC [5-10], although adenovirus (ADV)- and JC virus (JCV)-associated HC also occur: ADV type 11 is the prominent pathogen for HC, especially in Japan [11-17]. In general, primary ADV and BKV infections typically occur during childhood and remain latent in the genitourinary tract, but these viral infections are prevalent in allo-HSCT recipients and can cause viral-induced HC [1,2].

A number of retrospective studies have proposed a variety of risk factors for HC following allogeneic HSCT (allo-HSCT), including busulfan (BU)-containing myeloablative conditions, unrelated donors, and the occurrence of graft-versus-host disease (GVHD); however, these risk factors were not observed consistently. The analysis of risk factors is likely to be complicated by many variables, including the clinical definitions of HC, the HSCT protocols, or the number and age of patients analyzed. We performed a retrospective analysis of 42 Japanese adult allo-HSCT recipients with either ADV-HC (n = 26) or BKV-HC (n = 16), confirmed by polymerase chain reaction (PCR) examination, to identify risk factors for viral HC.

Table I. Pretransplantation Characteristics of the 266 Patients

Characteristics	Total	ADV-HC (n = 26)	BKV-HC (n = 16)	No-HC (n = 224)	P Value ADV versus No	P Value BKV versus No
Age, median (range)	48 (16-69)	48.5 (17-69)	52 (29-63)	46.5 (16-68)	.34	.21
Sex, male/female	152/114	17/9	11/5	124/100	.33	.3
Underlying disease					.004	.27
MDS/AML	106	5	10	91		
CML	11	1	1	9		
ALL	33	1	1	31		
ML	80	11	2	67		
AA	14	4	0	10		
Others	22	4	2	16		
Disease status at transplantation					.9	.011
Standard risk	123	13	1	109		
High risk	143	13	15	115		
Conditioning regimen					.93	.58
Conventional	134	13	7	114		
Reduced intensity	132	13	9	110		
Stem cell source					.66	.55
Related PB	69	6	6	57		
Related BM	14	3	0	11		
Unrelated BM	105	8	5	92		
Unrelated CB	64	7	5	52		
Haploidentical PB/BM	14	2	0	12		
Cycles of prior therapies, median (range)	5 (0-23)	4 (0-23)	4.5 (0-12)	5 (0-19)	.68	.79
Times of HSCT					.14	.5
1st	190	22	10	158		
≥2nd	76	4	6	66		
HLA matching					.6	.17
Full-matched	143	13	6	124		
Mismatched	123	13	10	100		
GVHD prophylaxis*					.61	.5
CsA-based	126	11	9	106		
FK-based	139	15	7	117		
In vivo T cell purging					.025	.8
Yes	19	5	0	14		
No	247	21	16	210		
IgG-antibody for ADV (titer)					.84	.26
≤ ×4	159	15	11	133		
×8	13	1	0	12		
×16	32	3	1	28		
Unknown	62	7	4	51		

MDS/AML indicates myelodysplastic syndrome/acute myelogenous leukemia; CML, chronic myelogenous leukemia; ALL, acute lymphoblastic leukemia; ML, malignant lymphoma; AA, aplastic anemia; PB, peripheral blood; BM, bone marrow; CB, cord blood; HSCT, hematopoietic stem cell transplantation; CsA, cyclosporine; FK, tacrolimus; GVHD, graft-versus-host disease; ADV, adenovirus; BKV, BK virus.
*One case that used only mPSL (methylprednisolone) was excluded.

PATIENTS AND METHODS

Patients

The medical records of 266 patients (152 men and 114 women; median age = 48 years), who underwent allo-HSCT at Kyushu University Hospital between January 2002 and June 2010, were reviewed; a subset of these patients has been described earlier [11]. Patient characteristics are listed in Table 1. Primary diseases included myelodysplastic syndrome (MDS)/ acute myeloid leukemia (AML; n = 106), chronic myelogenous leukemia (n = 11), acute lymphoblastic leukemia (ALL; n = 33), malignant lymphoma (n = 80), aplastic anemia (n = 14), and others (n = 22). Patients with any of the following conditions were classified as standard risk: acute leukemia (AML or ALL) in remission; chronic myelogenous leukemia in chronic phase; MDS classified as refractory anemia orrefractory

anemia with ringed sideroblasts. All others (n = 143) were categorized as high risk. This study was approved by the institutional review board of Kyushu University Hospital.

Transplantation Procedures

A total of 134 patients received conventional preparative regimens, either 12 Gy total body irradiation/CY (n = 94) or BU/CY (n = 40). The remaining 132 cases received purine analog-based reduced-intensity conditioning consisting of either fludarabine (Flu)/CY (n = 25), Flu/BU (n = 69), or Flu/melphalan (n = 38). Low-dose total body irradiation (2-4 Gy), antithymocyte globulin (ATG), and alemtuzumab were administered in 73, 14, and 4 cases, respectively (Table 1). The sources of stem cells included related granulocyte colony-stimulating factor-mobilized peripheral blood (n = 82), related bone marrow (n = 15), unrelated

bone marrow (n = 105), or unrelated cord blood (n = 64). Human leukocyte antigen (HLA)-matching varied from haploidentical (3 of 6) to identical (6 of 6). Of 266 patients, 126 and 139 received cyclosporine- or tacrolimus-based GVHD prophylaxis, respectively; the remaining 1 patient received methylprednisolone alone. A total of 76 patients had received at least 1 prior autologous (n = 28) or allogeneic (n = 48) HSCT, and the reason of second or more transplantations was either relapse (n = 65) or graft failure (n = 11) (Table 1). Acyclovir was given as prophylaxis against herpes simplex virus reactivation, 1000 mg/day orally from days −7 to 35 after HSCT.

Diagnosis and Treatment of Viral HC

Urinalysis was routinely performed at least once a week beginning with the initiation of preparative regimens until discharge or when clinical signs of cystitis appeared after that. If microscopic or macroscopic hematuria and/or bladder irritation existed, urine was further analyzed by rapid immunochromatography and PCR method to detect ADV antigen [11] or ADV, as well as BKV and JCV, viral DNA. Only patients with viruria confirmed by PCR were diagnosed with viral HC and included in our analysis.

All patients with viral HC were treated by supportive modalities including hyperhydration, forced diuresis, and/or blood transfusions. In addition, continuous bladder irrigation and/or administration of antiviral agents were performed based on each physician's decision. According to previous reports with a minor modification [9,10], the response criteria were defined as follows: complete response (CR), the complete resolution of HC symptoms accompanied by eradication of ADV or at least a 2-log reduction of BKV viral load; partial response (PR), a significant improvement of HC symptoms accompanied by persisting microhematuria or continued detection of ADV or BKV in the urine samples; and no change, no improvement or worsening of HC.

Statistical Analysis

The aim of this study was to identify factors correlating with the development of viral HC. Chi-square tests were used for univariate comparisons to examine categoric variables, including sex, underlying diseases, disease status, conditioning regimen, stem cell source, HLA matching, GVHD prophylaxis, and prior HSCT. A numerical variable (age) was compared using the Mann-Whitney test. Odds ratios (ORs) were calculated using a logistic regression analysis, and variables were analyzed using a multivariate stepwise logistic regression model. Survival following allo-HSCT was measured from the date of stem cell infusion until the date of death. The survival period was calculated

using the Kaplan-Meier method. P values <.05 were considered statistically significant. All statistical analyses were performed using SPSS 17.0 software (SPSS Japan Inc., Tokyo, Japan).

RESULTS

Incidence of Viral HC

In our series, a total of 42 of 266 allo-HSCT recipients (15.8%) developed viral HC. Of these, 26 (9.8%) were diagnosed with ADV-HC, including coinfection with BKV (n = 3) or JCV (n = 1), and 16 (6.0%) with BKV-HC alone. The immunochromatography assay for ADV antigen was positive in 20 of 24 tested urine samples of ADV-HC patients, although false-positive results were obtained in 4 of 13 BKV-HC patients, confirming the reliability of this assay for diagnosing ADV-HC [11].

ADV-HC has predominantly been reported from Japanese transplantation centers [11-17], whereas BKV-HC is frequently seen worldwide [5-10]. Because the role of BKV in HC pathogenesis remains unclear, because it is commonly found in the urine of unaffected patients, we analyzed ADV-HC and BKV-HC separately and compared it to patients without HC (n = 224).

Pretransplantation Characteristics of Patients with ADV-HC and BKV-HC

Six of 128 (4.7%) patients who underwent HSCT for acute leukemia (MDS/AML and ALL) developed ADV-HC, which was significantly less frequent than in the 20 of 122 (16.4%) patients suffering from other disorders (P = .004). A high incidence of ADV-HC was found in patients who received T cell purging using ATG or alemtuzumab (26.3%; 5 of 19) compared with those who did not (9.1%; 21 of 231; P = .025). Some studies have reported a close association between positive results of anti-ADV antibody and the development of ADV-HC [12,16], whereas another group [14] and our study could not detect such a relationship between them (Table 1). In contrast, BKV-HC was closely related to the status of underlying diseases at HSCT: high-risk patients developed BKV-HC more frequently than standard-risk patients (11.5%, n = 130 versus 0.9%, n = 110; P = .011). There was no association among viral HC with sex, stem cell source, or HLA matching. Moreover, the incidence of viral-HC was not affected by the usage of BU (BU-containing, 12.8%, n = 109 versus non-BU, 17.8%, n = 157; P = 0.27), usage of CY (CY-containing, 16.4%, n = 159 versus non-CY, 15.0%, n = 107; P = 0.76), or prior history of treatment (number of cycles of pretransplantation therapy) (Table 1).

Table 2. Clinical and Laboratory Manifestations of Viral-Associated HC

Case	Diagnosis	Graft	Conditioning	Preengraftment Allo-reaction	Maximum Grade of GVHD	Immunosuppressive Agents at HC Onset	Onset (Day)	Hematuria	Bladder Irritation	ADV-IC	Viruria (PCR)	Antiviral Agents	Response	CMV Reactivation	VZV Reactivation	Outcome
1	LPL	UBM	Conv	(−)	(−)	FK	2	macro	No	(+)	ADV	CDV	CR	(−)	(−)	survive
2	AA	RBM	RIC (ATG)	NA	NA	FK	4	macro	Yes	(+)	ADV	CDV	CR	NA	(−)	dead by infection
3	AA	RBM	RIC (Campath)	(−)	(−)	CsA	7	OB	No	(+)	ADV	CDV	CR	antigenemia	(+)	survive
4	ATL	UCB	Conv	NA	NA	CsA	7	macro	Yes	(−)	ADV	CDV + FCV	PR (viruria+)	NA	(−)	ATL relapse
5	ATL	UCB	RIC	HPS	(−)	FK	11	macro	No	(+)	ADV + BKV	CDV	PR (viruria+)	(−)	(−)	dead by bleeding
6	HPS	UCB	RIC (ATG)	(−)	(−)	FK/PSL	13	macro	Yes	(+)	ADV + BKV	CDV	PR (viruria+)	antigenemia	(−)	survive
7	ATL	RPB	Conv	PIR	acute(IV)	CsA/mPSL	19	OB	Yes	(+)	ADV	CDV	PR (OB+)	antigenemia	(−)	dead by infection
8	NK leukemia	UCB	Conv	(−)	(−)	CsA/PSL	22	macro	Yes	(+)	ADV	CDV + ribavirin	NC	antigenemia	(−)	survive
9	AA	haplo-BM	Conv	(−)	acute(II)	FK/PSL	25	macro	No	(+)	ADV	CDV	CR	antigenemia	(−)	survive
10	PTCL-u	UCB	RIC	(−)	(−)	FK	29	OB	Yes	(+)	ADV	GCV	CR	gastritis	(+)	survive
11	AA	UBM	RIC (ATG)	PIR	(−)	CsA	30	macro	Yes	(+)	ADV	CDV	PR (OB+)	antigenemia	(−)	dead by bleeding
12	AML	UBM	Conv	HPS	acute(II)	FK/PSL	31	macro	No	(+)	ADV	None	CR	antigenemia	(+)	dead by PD
13	NK lymphoma	RPB	RIC	PIR	acute(IV)	FK/mPSL	47	macro	Yes	(+)	ADV	CDV	CR	colitis	(−)	dead by TMA
14	MM	RPB	RIC	(−)	chronic(extensive)	CsA/PSL	79	OB	Yes	(+)	ADV	CDV	CR	antigenemia	(−)	survive
15	ATL	haplo-PB	RIC (ATG)	(−)	(−)	FK/PSL	120	macro	Yes	(+)	ADV	CDV	CR	antigenemia	(−)	survive
16	AML	UBM	Conv	(−)	(−)	FK	144	macro	Yes	(−)	ADV	CDV	CR	antigenemia	(−)	survive
17	AITL	UCB	RIC	PIR	acute(III)	CsA/PSL/MMF/ basiliximab	149	macro	No	NA	ADV	CDV	CR	antigenemia	(−)	dead by infection
18	MDS/AML	RPB	RIC	PIR	acute(II)	CsA/PSL	183	macro	Yes	(+)	ADV	CDV	PR (OB+)	antigenemia	(−)	dead by PD
19	MF	RPB	Conv	(−)	chronic (extensive)	CsA/PSL	184	macro	Yes	(+)	ADV	CDV	CR	(−)	(+)	survive
20	HCL	RPB	Conv	PIR	acute(II), chronic(limited)	CsA/PSL	265	OB	Yes	(+)	ADV	CDV	CR	(−)	(−)	survive
21	AML	RBM	Conv	(−)	acute(I), chronic (extensive)	CsA/PSL	266	macro	Yes	NA	ADV	None	CR	(−)	(−)	survive
22	CML	RBM	Conv	(−)	chronic(extensive)	PSL	281	macro	Yes	(+)	ADV	CDV	CR	antigenemia	(−)	survive
23	MF	UBM	RIC	(−)	(−)	FK/PSL	368	macro	Yes	(+)	ADV	CDV	CR	antigenemia	(−)	survive
24	AML	UBM	Conv	(−)	(−)	(−)	455	macro	Yes	(−)	ADV + JCV	None	PR (viruria+)	gastritis/colitis	(−)	dead by PD
25	ALL	UCB	RIC	(−)	(−)	(−)	484	macro	No	(+)	ADV	CDV	CR	(−)	(−)	survive
26	DLBCL	UBM	Conv	PIR	chronic(limited)	FK	875	macro	Yes	(−)	ADV + BKV	CDV	CR	antigenemia	(+)	survive
27	AML	UCB	RIC	HPS	(−)	CsA	6	OB	Yes	(+)	BKV	None	CR	antigenemia	(−)	dead by PD
28	ALL	UBM	Conv	PIR	acute(II)	FK	7	OB	Yes	(−)	BKV	None	PR (OB+)	antigenemia	(−)	dead by PD
29	Gastric Ca	RPB	RIC	HPS	NA	CsA/PSL	11	macro	No	(−)	BKV	None	NC	NA	(−)	dead by infection
30	DLBCL	UCB	RIC	PIR	acute(III)	CsA/PSL	29	macro	Yes	NA	BKV	None	NC	(−)	(−)	dead by PD
31	MDS/AML	UBM	Conv	(−)	acute(III)	FK/mPSL/MMF/ basiliximab	40	macro	No	NA	BKV	None	NC	antigenemia	(−)	dead by GVHD
32	ATL	UCB	RIC	PIR	acute(II)	CsA	42	macro	Yes	(−)	BKV	None	CR	antigenemia	(−)	dead by PD
33	MDS/AML	RPB	Conv	PIR	acute(II)	CsA/mPSL	44	OB	Yes	(−)	BKV	None	CR	antigenemia	(+)	dead by PD
34	MDS/AML	RPB	RIC	(−)	acute(II)	CsA/mPSL	49	macro	Yes	(+)	BKV	None	CR	antigenemia	(−)	dead by PD
35	MDS/AML	UBM	RIC	PIR	acute(II)	FK/mPSL	50	OB	Yes	(−)	BKV	None	CR	antigenemia	(−)	dead by PD

No.	Disease	Source	Conditioning	PIR/HPS	GVHD	Immunosuppression	Onset (day)	Hematuria	Macrohematuria/fever	aGVHD	Virus	Treatment	Response	Outcome
36	AML	UBM	Conv	PIR	acute(IV)	CsA/PSL	52	macro	No	(+)	BKV	CDV	PR (viruria+) (−)	dead by GVHD
37	AML	UCB	RIC	PIR	acute(III)	CsA	61	macro	Yes	(−)	BKV	CDV	PR (OB+) antigenemia	AML relapse
38	AML	UCB	Conv	PIR	(−)	CsA	66	macro	Yes	(−)	BKV	None	PR (OB+) antigenemia	dead by infection
39	MDS/AML	RPB	RIC	PIR	acute(II)	CsA/PSL	86	macro	No	(−)	BKV	CDV	PR (viruria+) antigenemia	survive
40	AML	RPB	Conv	HPS	chronic(limited)	CsA/PSL	122	macro	No	NA	BKV	CDV + Ara-A	PR (viruria+) antigenemia	dead by PD
41	Thymic Ca	RPB	RIC	(−)	acute(II), chronic(extensive)	CsA/PSL	134	macro	No	(−)	BKV	None	NC (−)	dead by PD
42	CML	UBM	Conv	PIR	chronic(extensive)	FK/PSL	443	macro	No	(+)	BKV	None	NC antigenemia	dead by renal failure

LPL indicates lymphoplasmacytic lymphoma; AA, aplastic anemia; ATL, adult T cell lymphoma; HPS, hemophagocytic syndrome; PTCL-u, peripheral T cell lymphoma unclassified; AML, acute myelogenous leukemia; MM, multiple myeloma; AITL, angioimmunoblastic T cell lymphoma; MDS, myelodysplastic syndrome; MF, myelofibrosis; HCL, hairy cell leukemia; CML, chronic myelogenous leukemia; ALL, acute lymphoblastic leukemia; DLBCL, diffuse large B cell lymphoma; UBM, unrelated bone marrow; RBM, related bone marrow; UCB, unrelated cord blood; RPB, related peripheral blood; Conv, conventional conditioning; RIC, reduced-intensity conditioning; ATG, antithymocyte globulin; NA, not assessed; PIR, preengraftment immune reaction; FK, tacrolimus; CsA, cyclosporin A; PSL, prednisolone; mPSL, methylprednisolone; MMF, mycophenolate mofetil; OB, occult blood; CDV, cidofovir; FCV, foscarnet; GCV, gancyclovir; CR, complete remission; PR, partial remission; NC, no change; VZV, varicella zoster virus; PD, progressive disease; TMA, thrombotic microangiitis; GVHD, graft-versus-host disease.

Clinical Findings of ADV-HC and BKV-HC

The clinical features of patients developing viral HC are shown in Table 2. The median onset of clinical symptoms was 49.5 days (range: 2-875 days), consistent with previous reports [13-15]. Most of the patients with ADV-HC (53.8%) and BKV-HC (75%) presented their symptoms more than 1 month after transplantation, indicating that viral HC was caused by the reactivation of latent infection rather than acute infection during the transplantation course. The frequency of macrohematuria or bladder irritation was similar between patients with ADV-HC and those with BKV-HC; however, the symptoms were more severe in ADV-HC.

At the onset of viral HC, almost all the patients were receiving immunosuppressive agents as either prophylaxis or treatment of GVHD or hemophagocytic syndrome (HPS). Interestingly, the incidence of allogeneic immune reactions was significantly different between patients with ADV-HC and BKV-HC. Acute GVHD (aGVHD) (maximum; grade II to IV) throughout the clinical course was marginally less frequent in ADV-HC patients than in patients without viral HC ($P = .054$; Table 3), possibly because of T cell purging. In contrast, patients with BKV-HC were more likely to have developed either noninfectious fever before engraftments known as a preengraftment immune reaction (PIR) [18] or HPS (80%) or postengraftment aGVHD (grade II-IV; 73.3%) than patients without viral HC (43.8%, $P = .013$ and 50.5%, $P = .099$, respectively; Table 3).

Finally, we found a significant or marginal increase of proven cytomegalovirus diseases (e.g. gastritis, colitis) or varicella zoster virus reactivation in ADV-HC patients compared with non-HC individuals (12.5% versus 3.6%, $P = .05$, and 20.8% versus 12.9%, $P = .29$, respectively).

Treatment and Outcome of Viral HC

In addition to supportive treatments, 8 of 46 patients with HC required continuous bladder irrigation. Twenty-two of 26 patients with ADV-HC and 4 of 16 patients with BKV-HC were treated with low-dose cidofovir (CDV; 1 mg/kg/day, 3 times a week), as previously reported [11]. In addition to CDV treatment, foscarnet was subsequently administered for 1 patient, ribavirin for 1, and Ara-A for the other because of their inadequate responses. Clinical features were relieved in all except 1 ADV-HC patient; 18 patients obtained CR, 7 obtained PR with persistent viruria (n = 4) or microhematuria (n = 3) without bladder irritation, and in the remaining case, autologous stem cell rescue for the primary graft failure improved his symptoms (case 8). Of the 16 patients with BKV-HC, symptoms persisted in 6 patients, although 5 of them did not receive antiviral agents because of either relapse of their

Table 3. Posttransplantation Characteristics of the 233 Engrafted Recipients

					P Value	
Characteristics	Total	ADV-HC (n = 24)	BKV-HC (n = 15)	No-HC (n = 194)	ADV versus No	BKV versus No
PIR and/or HPS					.56	*.013*
Yes	106	9	12	85		
No	127	15	3	109		
aGVHD*					*.054*	.099
No	89	16	4	69		
Grade I	28	1	0	27		
Grade II	79	4	7	68		
Grade III	25	1	3	21		
Grade IV	12	2	1	9		
CMV reactivation					.69	.47
Yes (antigenemia/diseases)	158/10	15/3	12/0	131/7		
No	65	6	3	56		
VZV reactivation					.29	.49
Yes	31	5	1	25		
No	202	19	14	169		

PIR indicates preengraftment immune reaction; HPS, hemophagocytic syndrome; aGVHD, acute graft-versus-host disease; CMV, cytomegalovirus; VZV, varicella zoster virus.
*Maximum grade throughout the observation period.
Statistically significant differences were indicated by italics.

underlying diseases, low performance status, or insufficient organ function (Table 2).

Nine of 26 patients with ADV-HC died because of infection (n = 4), disease progression (n = 3), and bleeding (n = 2). Of the surviving patients, 1 relapsed and 16 remained disease-free. In contrast, 14 of 16 patients with BKV-HC died because of disease progression (n = 9), other infection (n = 2), GVHD (n = 2), or renal failure (n = 1), and 1 patient relapsed, leaving a single disease-free survivor from the patients with this complication. In our study, the 1-year overall survival after HSCT was only 16.1% ± 10.2% for patients with BKV-HC, significantly lower than that of patients without HC (52.5% ± 3.4%) or with ADV-HC (63.7% ± 10.4%).

Risk Factors for ADV-HC and BKV-HC

Univariate analysis using logistic regression identified strong associations between ADV-HC and (1) the underlying disease (acute leukemia versus others; $P = .004$), (2) T cell purging ($P = .025$), and (3) less occurrence of severe aGVHD (grade II-IV versus grade 0-I; $P = .054$). Multivariate logistic regression analysis confirmed that all 3 factors had significant

or marginal association with developing ADV-HC; ORs were 4.488 (95% confidence interval (CI) = 1.625-12.40; $P = .004$), 4.176 (95% CI = 0.942-18.50; $P = .06$), and 0.390 (95% CI = 0.148-1.025; $P = .054$), respectively (Table 4).

Similar analysis of BKV-HC patients identified a significant relationship with disease status at HSCT (high risk versus standard risk; $P = .011$), PIR and/or HPS ($P = .013$), and marginal to aGVHD (grade II-IV versus grade 0-I; $P = .099$). Multivariate analysis showed that high-risk disease status (OR = 14.34; 95% CI = 1.81-113.4; $P = .012$) and presence of PIR and/or HPS (OR = 4.13; 95% CI = 1.06-16.14; $P = .041$) were the risk factors for BKV-HC (Table 4).

DISCUSSION

BKV is frequently isolated from asymptomatic patients before or following HSCT [5-8], and even from healthy individuals [19-21], indicating that the presence of BKV in urine samples is not always associated with HC. In contrast, ADV is almost exclusively detected in patients with HC, indicating a likely causative role [11-17,22]. BKV is more

Table 4. Results of Multivariate Logistic Regression Analysis

Characteristics		Odds Ratio (95% CI)	P Value
ADV-HC			
Underlying disease	Others versus acute leukemia	4.488 (1.625-12.40)	*.004*
In vivo T cell purging	Yes versus no	4.176 (0.942-18.50)	.06
aGVHD	grade II to IV versus 0 to I	0.390 (0.148-1.025)	.054
BKV-HC			
Disease status at transplantation	High risk versus standard risk	14.34 (1.812-113.4)	*.012*
PIR and/or HPS	Yes versus no	4.132 (1.058-16.14)	*.041*

Odds ratio were calculated by the backward or the forward stepwise selection methods.
Statistically significant differences were indicated by italics.

frequently detected in the urine of the posttransplantation patients compared with ADV, increasing from 7% to 47% for BKV and by 4% for ADV [6]. Despite a high BKV reactivation rate, HC occurs in only a fraction of patients with sustained BK viruria, whereas the majority of HSCT recipients with ADV viruria progress to HC [6,14,23]. In our study, we retrospectively analyzed 266 patients to identify the typical clinical features of Japanese adult allogeneic HSCT recipients who develop viral HC. The cumulative incidence of viral HC was 15.8% overall in our study group, 9.8% because of ADV and 6.0% because of BKV. We found that the factors associated with ADV- or BKV-HC were significantly different.

In the present study, approximately one-half of the ADV-HC cases were early onset (<1 month post-HSCT) and were closely associated with the underlying diseases including lymphoid malignancies and usage of ATG or alemtuzumab as a part of conditioning for AA patients, consistent with previous reports [22,24-26]. In contrast, late-onset ADV-HC (>1 month post-HSCT) was associated with chronic GVHD (6 of 14 patients) and the administration of prolonged immunosuppressants (12 of 14 patients; Table 2). In addition, 15 of 24 patients with ADV-HC were positive for the cytomegalovirus antigen test throughout HSCT, possibly indicating a general impairment of immune protection against viral reactivation. This suggests that profound immune suppression, such as T cell depletion or persistent GVHD and the resultant prolonged administration of immunosuppressants, may be a critical factor in the etiology of ADV-HC.

Only a subset of HSCT recipients with BK viruria progress to clinical BKV-HC, suggesting that other factors may be involved in this complication. Previous reports have shown that BKV-HC is extremely rare in autologous HSCT recipients [14,27,28], although their intensity of myeloablative preparative regimens, as well as the level and incidence of BK viruria, were similar among patients with autologous and allogeneic HSCT [27]. Here we have identified a significant association between occurrence of BKV-HC and aGVHD or non-T cell purging, consistent with previous reports from others [6,7,9,22,29]. Ten of 16 (62.5%) cases with BKV-HC developed their symptoms between engraftment and 100 days post-HSCT, in which aGVHD were frequently occurred, suggesting that immune reactions mediated by donor T cells may be an important contributing factor for developing BKV-HC. In addition, PIR and/or HPS, which are also indicative of excessive allogeneic immune reactions, were more frequently observed in patients with BKV-HC (80%, 12 of 15 patients) than among those without viral HC (43%, 85 of 194 patients). The lower frequency of severe aGVHD among

Japanese HSCT recipients than in Western countries [30,31] may, in part, account for the lower incidence of BKV-HC in Japan.

Our findings indicate that ADV- and BKV-HC may develop because of different mechanisms in allo-HSCT recipients. Although under normal circumstances, BKV and ADV remain latent in the urinary tracts following primary infection, analysis of urine samples using PCR indicates that BKV is able to replicate in healthy adults [19-21], although it does not typically lead to HC. BKV-HC was frequently found in patients with excessive allogeneic immune reactions such as GVHD, PIR, and HPS. Because BKV is usually not sufficient to cause HC, BKV might cooperate with excessive immune reactions to cause HC, although it remains unclear whether this immune attack can target the uroepithelium or not. In contrast, ADV is usually undetectable in the urine of healthy adults, indicating that ADV does not replicate under the normal immune status [32]. In the allo-HSCT recipients, ADV-HC was associated with T cell purging and the underlying disease. It is conceivable that severe immune suppression allows ADV replication to occur in the urinary tract, leading to local inflammation and subsequent development of HC. Because BKV viruria may be asymptomatic, it is likely that ADV is more virulent than BKV for developing HC.

The influence of HC on the outcome of HSCT remains controversial. In our study, 22 of 26 patients developing ADV-HC were promptly initiated low-dose CDV, as previously reported [11], resulting in CR in 15 patients and PR in 6 others, and the 1-year overall survival in patients with ADV-HC was similar to those without ADV-HC (63.7% versus 52.5%). In contrast, patients with BKV-HC had a very low probability of survival (<20%), although others have reported that the clinical course of BKV-HC was less severe than ADV-HC [6]. In these patients, the main cause of death was not the BKV-HC but the progression of the underlying diseases; 15 of 16 cases with BKV-HC underwent allo-HSCT against the uncontrolled diseases. Irrelevant immune reactions and the resultant administration of immunosuppressants might contribute to the reduction of the graft-versus-leukemia effect.

In conclusion, we have identified different related factors in HSCT recipients to develop either ADV-HC or BKV-HC, although there are the limitations to a retrospective, single-center analysis. Severe immunosuppression might play a pivotal role for ADV reactivation and subsequent development of ADV-HC, whereas an excessive immune reaction might be critical for the development of BKV-HC. Earlier diagnosis and intervention for ADV-HC with low-dose CDV therapy may provide a survival benefit. It will be interesting to see if these associations are found in other adult populations.